Efficient *ab initio* method for inelastic transport in nanoscale devices: Analysis of inelastic electron tunneling spectroscopy

Hisao Nakamura* and Koich Yamashita
Department of Chemical System Engineering, Graduate School of Engineering, The University of Tokyo, Tokyo 113-8656, Japan

Alexandre. R. Rocha and Stefano Sanvito
School of Physics and CRANN, Trinity College, Dublin 2, Ireland

(Received 30 July 2008; revised manuscript received 20 October 2008; published 11 December 2008)

We describe the *ab initio* nonequilibrium Green's function method for electron-transport calculations in nanoscale devices based on the "efficient molecular-orbital approach." This is implemented in the density-functional theory code SIESTA with the additional option of including effects originating from electron-phonon coupling. We also derive simple expressions for the conductance and the inelastic electron tunneling spectrum (IETS) based on the rigorous lowest-order expansion formalism. In order to illustrate our method, we have performed calculations of inelastic transport in a linear gold atomic wire and a benzene-dithiol molecule both sandwiched between gold electrodes. In the latter case the leads have been constrained to maintain an overall D_{2h} symmetry, as typical of both high- and low-conductance systems. The shapes of the IETS, the effect of the temperature, and of the symmetry of the IETS signals are analyzed in details.

DOI: 10.1103/PhysRevB.78.235420 PACS number(s): 72.10.Di, 68.37.Ef, 73.63.Rt

I. INTRODUCTION

Electron transport in single molecules or in atomic wires connected to bulk electrodes, to which we refer shortly as electrode-molecule-electrode (E-M-E) systems, has attracted great interest because of the prospect for applications as new nanoscale devices.[1] Experimental studies have succeeded in measuring the *I-V* characteristics[2–4] and reported nonlinear properties of the *I-V* curves as the result of negative differential resistance for several groups of molecules.[5–7] These studies have shown the possibility of constructing functional devices. Generally, it is difficult to manipulate, define, and characterize with atomic accuracy the experimental contact region between the molecule and the electrodes; hence theoretical studies based on *ab initio* calculations for realistic E-M-E models, which explicitly contain the nanoscale contacts and semi-infinite electrodes, are highly desirable and useful.[1,8,9] Density functional theory (DFT) is among the most convenient approaches for treating nanoscale systems and offers an atomistic description without the need of system-specified parameters. However, the application of DFT to electron transport in E-M-E systems is not straightforward because of the nonequilibrium open boundary conditions caused by the existence of the electrodes and the applied bias voltage.

The nonequilibrium Green's function (NEGF) formalism is often adopted to overcome such difficulties, and it has been combined with DFT (NEGF-DFT) to yield a practical method for calculations.[10–18] Several groups have recently developed NEGF-DFT computational codes, and these have been applied to E-M-E systems.[10,14–16,19] However, the standard scheme of the NEGF-DFT requires an estimation of a large Green's function matrix (GFM), the computational cost of which is very high for the self-consistent field (SCF) calculation required by the method. From now on we will call such scheme NEGF-SCF. For instance, one can point to difficulties in convergence and numerical instabilities in the integration of the lesser Green's function when the E-M-E system has a large bridge molecule or the system shows low coverage.

In the development of nanoscale devices the interaction between electrons and nuclear vibrations (phonons) is another central issue.[2,20–22] For electron transport in E-M-E systems, the electron-phonon (e-ph) interaction is important and it leads to inelastic current as well as to corrections to the elastic one.[12,22–26] As a consequence, e-ph interaction affects various characteristics of the devices, such as their conductance. Inelastic transport in molecular junctions is also interesting as a spectroscopic tool. For instance the inelastic electron tunneling spectroscopy (IETS) allows us to measure single adsorbed molecule vibrational spectra, and it can be used both theoretically and experimentally to deduce information about an adsorbate or the atomic details of a nanoscale junction.[24,27–35] Furthermore, the vibrational heating, caused by nonthermal phonon excitations due to e-ph interactions (where the phonons are not distributed according to the Bose-Einstein statistic), can trigger chemical reactions on surfaces. Hence the local control of nonthermal heating is a promising technique to perform chemistry controlled at the single molecule level.[29,36–39]

The NEGF method is formally extendable to both electrons and phonons. The transport process can be expressed using electron and phonon Green's functions coupled to each other through e-ph self-energy terms.[40] Although it is difficult to construct a general scheme for calculating the e-ph self-energies, practical approximations exist in some cases. When e-ph interaction is weak and the transit time through the contact is sufficiently short (i.e., off-resonant to phonon modes), the lowest-order perturbation theory (LOPT), which is the second-order perturbation expansion of the total current for the electron-phonon couplings, or the Born approximation (BA) may be good starting points.[30,41,42] However, Galperin *et al.*[24] recently performed simple model calculations and pointed out that the LOPT cannot reproduce the

shape of IETS and the BA has some shortcomings, e.g., no conservation of current, etc. The self-consistent Born approximation (SCBA) is a valid response to the above-mentioned problems,[12,42,43] but it is not a very practical scheme for *ab initio* calculations since it has a much higher computational cost than standard NEGF-SCF calculations nonincluding e-ph interaction. First, the SCF calculation shows more difficulty in converging because the SCBA procedure requires the simultaneous determination of both electron and phonon Green's functions through e-ph self-energy terms. Usually the lesser phonon Green's function changes rapidly when the bias is close to an eigenmode frequency. Second, a large number of energy grid points must be taken into account in order to estimate the e-ph self-energies. Furthermore, NEGF calculations should be performed at each applied voltage with very small increments if one needs to evaluate the details of the IETS (when these are rather narrow in energy).

Recently, Frederiksen and co-workers[23,25,44] proposed an alternative approach named the lowest-order expansion (LOE) approach. The LOE has the same form with the lowest-order BA for the expression of the current. Then the relating self-energies are expanded in the second order of electron-phonon couplings, which consist of zero-order electron Green's functions and the second-order phonon Green's functions constructed by electron-phonon self-energy terms for phonon. The obtained phonon Green's functions include the contribution of (nonthermal) vibrational heatings, and the resulting current by the LOE consists of the higher order terms than the second order of electron-phonon couplings. More recently, Viljas *et al.*[26] derived a rigorous LOE expression. Comparing the standard BA, the LOE has a few merits with maintaining preferable features of BA or SCBA for our purpose. The first is the current conservation, which is proofed in Ref. 26. The second is that the nonequilibrium phonon is easily accounted for with the same order with the electron, i.e., the second order of electron-phonon couplings.

One of the most important features of IETS is the relation between its shape and the magnitude of the conductance. It is well known that in many cases, the shape of the IETS changes from a peak to a dip on increasing the ballistic electron-transmission coefficients. This is sometimes called the "0.5 rule"[24,27,35] with the meaning that a peak (dip) appears in the IETS when the elastic transmission coefficient at that energy is smaller (larger) than 0.5. Recent theoretical studies gave clear analyses of the 0.5 rule, but they are limited to a model system comprising a single (resonant) level in the contact.

The symmetry properties of the IETS signals form another important issue since they provide selection rules for the individual molecular vibrations.[31] In addition, establishing the symmetry rules of the IETS will be also important in designing a functional nanodevice because the IETS activities can be a useful tool to visualize an actual electronic pathway in the bridge molecule.[45] Although several theoretical analyses have been performed in this context, some of these studies adopt simplified models such as the cluster model, focusing only on the totally symmetric normal modes[46] or have been performed within the BA,[33,41,47,48] where the phonon distribution is fixed with thermal equilibrium and vibrational heatings are often omitted. Therefore, there are some rooms for analyzing E-M-E systems that maintain high symmetry with the more rigorous *ab initio* calculations based on the LOE framework.

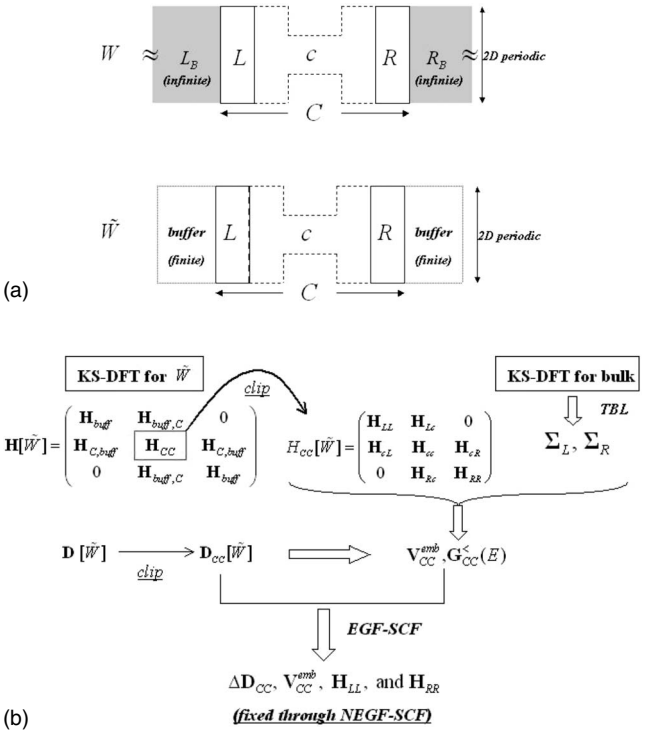

FIG. 1. (a) The schematic picture of our two generic systems W and $\tilde{W}$. In the transport setup, the device part is the C region, which consists of the left (L) and right (R) lead parts and the central bridge (c) regions. The two leads are connected to *infinite* bulk denoted as L_B and R_B, and the Hamiltonian in Eq. (1) is defined for this W. Note that the W is realistic but impossible to be calculated exactly. The $\tilde{W}$ is a model system for W, which replaces the L_B and L_R parts to finite-size buffer layers. The Hamiltonian and density matrix in the C region of W can be described by KS-SCF calculation for result for the supercell $\tilde{W}$ when the system is under equilibrium. (b) The flow chart of the preliminary procedure in the efficient MO approach. The procedure consists of calculations of embedding potential, self-energies, EGF-SCF, and corrected density matrix. Recall that we need only the matrices on the C region after the preliminary procedure, and the elements in the buffer part of $\tilde{W}$ are never used.

In our previous work, we proposed an efficient scheme for a self-consistent NEGF-DFT method based on molecular-orbital (MO) theory, designated as the "efficient MO approach."[13] This comprises three features, namely, (a) the use of an embedding potential, (b) the perturbative expansion of GFMs over the MO basis, and (c) a restricted MO space during the NEGF-SCF steps. The efficiency of our scheme is demonstrated by analyzing a few test cases. In this paper, we present several modifications and improvements to our efficient MO approach. These consist of (i) an improvement in how the embedding potential is constructed, (ii) the introduction of a numerically more accurate estimation of the density matrix with a correction factor, and (iii) a correct $O(N)$ algorithm to calculate the self-energy matrix of the electrodes.

Furthermore, we introduce a conventional form to analyze the shape of the IETS within the LOE framework and apply it to realistic E-M-E systems.

The paper is organized as follows. In Sec. II we provide a brief review of the NEGF formalism including e-ph interaction and a conventional LOE formula to be used in the present study. Then, in Sec. III, we outline our NEGF-SCF algorithm with details of the improvements in the method mentioned above. A summary discussion of our scheme is also given. Test calculations for two systems, an atomic gold wire and a benzene-dithiol (BDT) molecule both contacted with gold electrodes, are presented in Sec. IV. Finally our conclusions are drawn in Sec. V.

II. NEGF FORMALISM

A. Theoretical background

In order to model transport in E-M-E systems, only the device part (the region where the electrostatic potential differs from that of the bulk electrodes), which we denote as C, is explicitly considered, while the semi-infinite electrodes, which are labeled as L_B (left) and R_B (right), are renormalized by self-energy terms. For later use, we *symbolically* denote the whole device, which includes the entire semi-infinite L_B, R_B parts, and C as W. As standard, we further divide the C region into three parts: the L, R, and c regions. Here L and R are regarded as the left-hand and right-hand side leads; thus the self-energy terms are added to these L and R regions. c is the center region, which relates to the junction and includes a bridge molecule or wire and a few surface layers, and is usually updated by the SCF procedure in the NEGF-SCF calculations. A pictorial representation of those partitions is presented in Fig. 1(a). First, let us introduce the Hamiltonian for the electrons coupled to vibrational modes as follows:

$$
\begin{aligned}
H &= H^{\mathrm{e}} + H^{\mathrm{ph}} + H^{\text{e-ph}}, \\
H^{\mathrm{e}} &= \sum_{m,m'} (H_{CC})_{mm'} d_m^\dagger d_{m'} + \sum_{ii'} (H_{L_B L_B})_{ii'} c_i^\dagger c_{i'} \\
&\quad + \sum_{jj'} (H_{R_B R_B})_{jj'} c_i^\dagger c_{i'} + \left[\sum_{mi} (H_{CL_B})_{mi} d_m^\dagger c_i \right. \\
&\quad \left. + \sum_{mj} (H_{CR_B})_{mj} d_m^\dagger c_j \right] + [\mathrm{H.c.}], \\
H^{\mathrm{ph}} &= \sum_{\alpha} \Omega_\alpha b_\alpha^\dagger b_\alpha, \\
H^{\text{e-ph}} &= \sum_{\alpha,m,m'} M^{\alpha}_{mm'} d_m^\dagger d_{m'} (b_\alpha^\dagger + b_\alpha), \qquad (1)
\end{aligned}
$$

where $d^\dagger$ and $c^\dagger$ are creation operators for an electron in the C region and in the electrodes, respectively. The terms $(H_{CC})_{mm'}$, $(H_{L_B L_B / R_B R_B})_{ii'}$, and $(H_{CL_B / CR_B})_{mi}$ are the matrix elements of the mean-field Hamiltonian expressed over an atomic-orbital (AO) basis set, respectively, in the C region, the electrodes (bulk), and the transfer integrals. The operator $b_\alpha^\dagger$ is the phonon creation operator associated to the vibrational mode α, with frequency Ω_α, and the e-ph coupling is denoted as $M^{\alpha}_{mm'}$. In the present study, we consider e-ph interaction only in the C region; hence the coupling term $M^{\alpha}_{mm'}$ is defined only in C.

We start by describing the NEGF framework in the practical matrix form for ballistic transport, i.e., without e-ph interaction. In matrix form, the electron GFM in the C region can be written using an explicit block matrix

$$
\mathbf{G}^0_{CC}(E) = \begin{pmatrix} E\mathbf{S}_{LL} - \mathbf{H}_{LL} - \mathbf{\Sigma}_L(E) & E\mathbf{S}_{Lc} - \mathbf{H}_{Lc} & 0 \\ E\mathbf{S}^\dagger_{Lc} - \mathbf{H}^\dagger_{Lc} & E\mathbf{S}_{cc} - \mathbf{H}_{cc} & E\mathbf{S}_{cR} - \mathbf{H}_{cR} \\ 0 & E\mathbf{S}^\dagger_{cR} - \mathbf{H}^\dagger_{cR} & E\mathbf{S}_{RR} - \mathbf{H}_{RR} - \mathbf{\Sigma}_R(E) \end{pmatrix}^{-1}, \qquad (2)
$$

where the superscript "0" in G^0_{CC} indicates that there is no e-ph interaction. $\mathbf{S}$ is the overlap matrix between the AO basis functions and the units $\hbar = e = 1$ are used. Here, we assume that the direct interaction between the L and R regions is negligible, and this is justified by the use of the AO basis as long as the central region is sufficiently large. The semi-infinite electrodes connected to bulk L_B/R_B are renormalized by the lead self-energy terms $\Sigma_{L/R}(E)$.

When constructing $\mathbf{G}^0_{CC}(E)$ under the finite bias V_b, an external potential V_{ext}, which satisfies the appropriate boundary conditions at the L and R regions, should be added to $\mathbf{H}_{CC}$. In addition, the lead self-energies $\Sigma_{L/R}(E)$ must be shifted to $\Sigma_{L/R}(E \pm \frac{V_b}{2})$ in order to incorporate the above boundary conditions. The lesser Green's function, $G^<(E)$, and greater Green's function, $G^>(E)$, can be calculated in a matrix form using the Keldysh-Kadanoff-Baym (KKB) equations[40,49,50]

$$
\begin{aligned}
\mathbf{G}^{0<}_{CC}(E) &= \mathbf{G}^0_{CC}(E)[\mathbf{\Sigma}^<_L(E) + \Sigma^<_R(E)]\mathbf{G}^{0\dagger}_{CC}, \\
\mathbf{G}^{0>}_{CC}(E) &= \mathbf{G}^0_{CC}(E)[\mathbf{\Sigma}^>_L(E) + \mathbf{\Sigma}^>_R(E)]\mathbf{G}^{0\dagger}_{CC}, \qquad (3)
\end{aligned}
$$

where the lesser and greater self-energies relating to electron (hole) transport from (to) electrodes are written as follows:

$$
\mathbf{\Sigma}^<_L(E) + \mathbf{\Sigma}^<_R(E) = i f_L(E) \mathbf{\Gamma}_L\left(E + \frac{V_b}{2}\right) + i f_R(E) \mathbf{\Gamma}_R\left(E - \frac{V_b}{2}\right),
$$

$$\boldsymbol{\Sigma}_L^>(E) + \boldsymbol{\Sigma}_R^>(E) = i\{f_L(E) - 1\}\boldsymbol{\Gamma}_L\left(E + \frac{V_b}{2}\right) + i\{f_R(E) - 1\}\boldsymbol{\Gamma}_R\left(E - \frac{V_b}{2}\right). \quad (4)$$

The terms $\Gamma_{L/R}(E)$ are $i[\Sigma_{L/R}(E) - \Sigma_{L/R}^\dagger(E)]$, and $f_{L/R}(E)$ are the Fermi distribution functions with the Fermi level $\mu_{L/R}$. Since the density matrix $\mathbf{D}_{CC}$ is the energy integral of the lesser GFM, the GFMs are determined self-consistently through an updated $\mathbf{H}_{CC}$, where in the NEGF-DFT scheme the Hamiltonian is the Kohn-Sham (KS) Hamiltonian.

The ballistic current, I^0, can be formally expressed as a function of V_b once the GFM has self-consistently converged

$$I^0(V_b) = \frac{1}{\pi}\int dE\ \mathrm{Tr}[\boldsymbol{\Sigma}_L^<(E)\mathbf{G}_{CC}^{0>}(E) - \boldsymbol{\Sigma}_L^>\mathbf{G}_{CC}^{0<}(E)]. \quad (5)$$

This can be further simplified to yield the Landauer-Buttiker formula[51] using the transmission coefficient T_0 as follows:

$$\begin{aligned} I^0(V_b) &= \frac{1}{\pi}\int dE\ \mathrm{Tr}[\boldsymbol{\Gamma}_L(E + V_b/2)\mathbf{G}_{CC}^0(E)\boldsymbol{\Gamma}_R(E - V_b/2) \\ &\quad \times \mathbf{G}_{CC}^{0\dagger}(E)][f_L(E) - f_R(E)] \\ &= \frac{1}{\pi}\int dE T_0(E, V_b)[f_L(E) - f_R(E)] \sim G_0 T_0(E_F, 0)V_b, \end{aligned} \quad (6)$$

where the last equation is often used at low bias because of its convenience. The term G_0 is the conductance unit $\frac{e^2}{\pi\hbar}$, which equals $\frac{1}{\pi}$ in the present units, and E_F is the Fermi energy. In this study, we include a factor 2 accounting for spin degeneracy (we do not consider spin-polarized systems).

Next, we extend this formalism to inelastic transport by including $H^{\text{e-ph}}$. The e-ph interaction can be also renormalized (as the presence of the electrodes) by using the e-ph self-energies $\Sigma_{\text{e-ph}}^<$ and $\Sigma_{\text{e-ph}}$. When phonon-phonon coupling between different modes is negligible, the above self-energies are simply the sum of the self-energies of each individual mode, i.e., $\Sigma_{\text{e-ph}}^< = \Sigma_\alpha \Sigma_{\alpha:\text{e-ph}}^<$ and $\Sigma_{\text{e-ph}} = \Sigma_\alpha \Sigma_{\alpha:\text{e-ph}}$.[12,26,32,43] Since the e-ph interaction also leads to a nonequilibrium phonon distribution, the phonon Green's functions for the mode α, D_α and $D_\alpha^<$ are required:

$$D_\alpha(\omega) = \frac{2\Omega_\alpha}{\omega^2 - \Omega_\alpha^2 + i\eta - 2\Omega_\alpha \Pi_{\text{e-ph}:\alpha}(\omega)},$$

$$D_\alpha^<(\omega) = D_\alpha \Pi_{\text{e-ph}:\alpha}^< D_\alpha^\dagger, \quad (7)$$

where $\Pi_{\text{e-ph}:\alpha}^<$ and $\Pi_{\text{e-ph}:\alpha}$ are e-ph self-energies of the phonon. The parameter η is a broadening parameter and describes the couplings between the mode α and a phonon bath located in the electrodes, and it is responsible for phonon dissipation. The lesser Green's function, $D_\alpha^<(\omega)$, corresponds to the phonon distribution function $N_\alpha(\omega)$ and reads as follows:

$$D_\alpha^<(\omega) = 2iN_\alpha(\omega)\mathrm{Im}\ D_\alpha \quad (\omega > 0),$$

$$D_\alpha^<(\omega) = -2i[1 + N_\alpha(-\omega)]\mathrm{Im}\ D_\alpha \quad (\omega < 0). \quad (8)$$

Then the phonon occupation for the mode α can be approximately estimated by $N_\alpha(\Omega_\alpha)$.

The electron GFM, $\mathbf{G}_{CC}$, is then obtained by including $\boldsymbol{\Sigma}_{\text{e-ph}}(E)$ in the Dyson equation, and $\mathbf{G}_{CC}^<$ is also obtained by adding $\boldsymbol{\Sigma}_{\text{e-ph}}^<(E)$ to the KKB equation. When the e-ph coupling and the energy barrier height V_h at the interface (junction) satisfy the following condition:[52]

$$|M^\alpha| \ll (\Delta V_h^2 + \Gamma_{L/R}^2)^{1/2}, \quad (9)$$

then the e-ph interaction may be treated as a weak perturbation. In this case, the e-ph self-energies can be estimated from the lowest-order diagram (second order in M^α) and they are obtained by a convolution integral, which includes the terms M^α, $G_{CC}^\lessgtr$, G_{CC}, $D_\alpha^\lessgtr$, and D_α. Since the electron and phonon Green's functions are coupled to each other through the self-energies, one can solve the coupled Dyson and KKB equations self-consistently in the BA framework, i.e., all Green's functions should be simultaneously determined. This is the SCBA. Although the SCBA has various advantages when compared to the second-order Born expansion or the LOPT,[24] practical first-principles calculations for large molecules or low-coverage systems (i.e., where the cell describing the terminal interface is large) are complicated by the high computational cost. This is because the SCBA includes convolution integrals of both the electron and phonon energies and one needs to calculate the Green's functions on fine energy grids. A detailed analysis of the computational efficiency for the SCBA is discussed in Appendix B of Ref. 12. Furthermore, results obtained with SCBA calculations are usually not very convenient for a detailed analysis of the various contributions of e-ph scattering to inelastic transport. Recently, the LOE framework, which is an extension of the second-order perturbation expansion, has been proposed. The LOE expression can reproduce the shape of the IETS obtained by the SCBA and gives clear relations between the current and the relative ratio between elastic and inelastic e-ph scatterings. In Sec. II B, we present a simple formulation for calculating the conductance and the IETS for inelastic transport based on the LOE framework.

B. Conventional LOE formulation

As stated in Sec. I briefly, the LOE approach is formally a simplification of the BA expansion, but it provides a practical way to reproduce a correct shape of IETS and to estimate vibrational heatings consistently with the nonequilibrium electrons without self-consistent calculations. Furthermore it is convenient to carry out physical analysis by decomposing the current into ballistic I^0, elastic correction δI^{el}, and inelastic I^{inel} terms although it is only qualitative and not a unique feature of the LOE. A rigorous formulation of the LOE approach was derived already by Viljas *et al.*,[26] but practical *ab initio* calculations of IETS have been performed only using simplified LOE equations.[23,25] In the present study, we propose the conventional LOE formulations for estimating terminal currents and IETS signals assuming that (1) weak electron-phonon coupling limit and (2) the density of states

(DOS) for leads should be sufficiently smooth functions of E in the region close to the focused Ω_α, and the reader should keep in mind the limitation of our LOE approach. Note that this limitation is similar to the more simplified LOE,[23,25] and the recent study shows the limitation relating to the DOS is sometimes relaxed for a practical use.[12]

The total current is expressed as the sum of I^0, δI^{el}, and I^{inel}, i.e.,

$$I = I^0 + \delta I^{\mathrm{el}} + I^{\mathrm{inel}}. \tag{10}$$

Each term in the current can be obtained by integration of the terminal current, $i^0(E)$, $\delta i^{\mathrm{el}}(E)$, and $i^{\mathrm{inel}}(E)$. For instance, the ballistic terminal current can be expressed as

$$i^0(E) = \frac{1}{\pi} T_0(E)[f_L(E) - f_R(E)]. \tag{11}$$

Since the rigorous LOE formulation contains an integration over the phonon energy, the calculation requires the estimation of the terminal current for each energy E. As a result, the computational cost is still high. Thus the rigorous LOE expression may be not sufficiently practical for *ab initio* calculations, just as the SCBA. Furthermore, the energy dependence of the terminal current is sometimes important in the analysis of the conductance as well as the energy transfer due to electron-phonon scattering. Therefore, we propose a simple LOE expression, which requires the same computational cost as the ballistic terminal current but it is more accurate than the previous simplest LOE, where any energy dependence in the Green's functions is neglected and fixed with the value at the Fermi level. In order to achieve this, we introduce two approximations: (i) we take the 0 limit for η and $\Pi_{\text{e-ph:}\alpha}$ in the integrals and (ii) we omit the energy shift by Ω_α when evaluating the Green's functions. The first approximation relates to the delta function approximation for the imaginary part of the phonon Green's function and it is usually valid because the broadening factor for the phonon Green's functions is not very large when compared to the typical numerical energy grid spacing. The second approximation is acceptable as long as the density of states or the transmission coefficient does not feature a sharp peak at $E \sim \Omega_\alpha$, which is consistent with our fundamental assumption to introduce the conventional LOE. The detailed expressions are given in the Appendix.

In order to represent details of the shape of the IETS, the nonequilibrium phonon distribution should be evaluated. Equation (8) shows that this is obtained from lesser phonon Green's function. Since we introduce the approximation (ii), it is sufficient to estimate $D^<_\alpha(\Omega_\alpha)$. When the broadening parameter η is sufficiently large, one can assume that the energy transfer to the phonon bath (phonon dissipation) is very fast and thermal equilibrium is always established. To incorporate this aspect, $\Pi^<_{\text{e-ph:}\alpha}(\Omega_\alpha)$ in Eq. (7) is slightly modified as $\Pi^<_{\text{e-ph:}\alpha}(\Omega_\alpha) - i\eta N_{\mathrm{BE}}(\Omega_\alpha, T)$, where N_{BE} is the Bose-Einstein distribution function and T is the temperature of the substrate (electrodes). Then we can obtain the term $N_\alpha(\Omega_\alpha)$ from $\Pi^<_{\text{e-ph:}\alpha}(\Omega_\alpha)$ and $\Pi_{\text{e-ph:}\alpha}(\Omega_\alpha)$ as follows:

$$N_\alpha(\Omega_\alpha) = \frac{1}{2} \frac{\mathrm{Im}\,\Pi^<_{\text{e-ph:}\alpha}(\Omega_\alpha) - \eta N_{\mathrm{BE}}(\Omega_\alpha, T)}{\mathrm{Im}\,\Pi_{\text{e-ph:}\alpha}(\Omega_\alpha) - \eta/2}. \tag{12}$$

Although we omit phonon-phonon interactions, the dissipation of the mode α caused by the coupling to bath modes in electrodes is incorporated via the broadening parameter in Eq. (12). In Eq. (12), setting the parameter η to 0 gives the "externally undamped limit," i.e., the efficiency of the vibrational current induced heating is 100% (phonons generated in the scattering region are never dissipated). In contrast, if η is set to $\eta \to \infty$, a given mode couples with the heat bath (bath modes in electrodes) and it is in thermal equilibrium. This is the "externally damped limit." Usually, η has a finite value, and therefore the vibrational heatings generated by inelastic transport and dissipation are competing.[26] The calculation of η is a complicated issue that requires the solution of dynamical equations for all of the phonon modes and their couplings. In practice it can be estimated by fitting the DOS of phonon (Ref. 12) though we do not adopt this fitting procedure in the present study and we leave it as a free parameter.

One can obtain the total conductance, G, or the IETS, $\frac{dG}{dV_b}$, by numerical differentiation of the calculated I-V curves. However, in the usual IETS experimental situation, the applied voltage is low; thus the derivatives of terms including only $\mathbf{G}^0_{CC}$, $\mathbf{\Gamma}_{L/R}$, and $\mathbf{M}^\alpha$ with respect to V_b are negligible when compared to the derivatives of the functions $\frac{df_{L/R}}{dV_b}$ and $\frac{dN_\alpha(\Omega_\alpha)}{dV_b}$. As a result, one obtains simpler and numerically more convenient formulas for the conductance and the IETS as follows:

$$\begin{aligned} G(V)/G_0 = \bar{T}_0 + \sum_\alpha \Bigg\{ & \bar{T}^{\mathrm{ec}}_\alpha (2N_\alpha + 1) + 2\bar{T}^{\mathrm{ec}}_\alpha \frac{dN_\alpha}{dV_b} V_b \\ & - \bar{T}^{\mathrm{ecSym}}_\alpha + \bar{T}^{\mathrm{ecSym}}_\alpha \frac{dF_\alpha}{dV_b} \Bigg\} \\ & + \sum_\alpha \left\{ 2\bar{T}^{\mathrm{in}}_\alpha N_\alpha(\Omega_\alpha) + 2\bar{T}^{\mathrm{in}}_\alpha \frac{dN_\alpha}{dV_b} V_b + \bar{T}^{\mathrm{in}}_\alpha \frac{dF_\alpha}{dV_b} \right\}, \end{aligned} \tag{13}$$

$$\begin{aligned} \frac{1}{G_0}\frac{dG}{dV_b} = & \sum_\alpha \left\{ 4(\bar{T}^{\mathrm{ec}}_\alpha + \bar{T}^{\mathrm{in}}_\alpha) \frac{dN_\alpha}{dV_b} + 2(\bar{T}^{\mathrm{ec}}_\alpha + \bar{T}^{\mathrm{in}}_\alpha) \frac{d^2 N_\alpha}{dV_b^2} \right\} \\ & + \sum_\alpha \left\{ (\bar{T}^{\mathrm{ecSym}}_\alpha + \bar{T}^{\mathrm{in}}_\alpha) \frac{d^2 F_\alpha}{dV_b^2} \right\}, \end{aligned} \tag{14}$$

where F_α is the analytic function

$$\begin{aligned} F_\alpha(V_b, T) = & (\Omega_\alpha - V_b) N_{\mathrm{BE}}(\Omega_\alpha - V_b, T) \\ & + (\Omega_\alpha + V_b) N_{\mathrm{BE}}(\Omega_\alpha + V_b, T) \end{aligned} \tag{15}$$

and $\bar{T}$ represents the averaged transmission functions $T(E)$ as a function of energy E in the range $[\mu_R, \mu_L]$. The transmission functions $T^{\mathrm{ec}}_\alpha(E)$, $T^{\mathrm{ecSym}}_\alpha(E)$, and $T^{\mathrm{in}}_\alpha(E)$ can be taken from Ref. 26 and read

$$T_\alpha^{\mathrm{ec}}(E) = 2\ \mathrm{Re}\ \mathrm{Tr}[M^\alpha \mathbf{G}_{CC}^0(E) M^\alpha \mathbf{G}_{CC}^0(E) \mathbf{\Gamma}_R(E - V_b/2) \times \mathbf{G}_{CC}^{0\dagger}(E) \mathbf{\Gamma}_L(E + V_b/2) \mathbf{G}_{CC}^0(E)], \quad (16)$$

$$T_\alpha^{\mathrm{ecSym}} = 2\ \mathrm{Im}\ \mathrm{Tr}[\mathbf{M}^\alpha\ \mathrm{Im}\ \mathbf{G}_{CC}^0(E) \mathbf{M}^\alpha \mathbf{G}_{CC}^0(E) \mathbf{\Gamma}_R(E - V_b/2) \times \mathbf{G}_{CC}^{0\dagger}(E) \mathbf{\Gamma}_L(E + V_b/2) \mathbf{G}_{CC}^0(E)], \quad (17)$$

$$T_\alpha^{\mathrm{in}}(E) = \mathrm{Tr}[\mathbf{M}^\alpha \mathbf{G}_{CC}^0(E) \mathbf{\Gamma}_R(E - V_b/2) \mathbf{G}_{CC}^{0\dagger}(E) \mathbf{M}^\alpha \mathbf{G}_{CC}^{0\dagger}(E) \times \mathbf{\Gamma}_L(E + V_b/2) \mathbf{G}_{CC}^0(E)]. \quad (18)$$

In the present study, we adopt an *atomic on-site* Holstein type model for the entire C region,[53,54] which includes both local and nonlocal couplings. Thus the matrix is expanded in the AO basis. Then it can be transformed in the MO basis if required. As discussed in the following sections, the MO basis is useful for the analysis of e-ph coupling and the symmetry of the IETS. Therefore, at this time it is useful to provide the matrix form in the MO basis

$$M_{IJ}^\alpha = \sum_\mu \left(\langle I | \frac{\partial H}{\partial R_\mu} | J \rangle - \varepsilon_J^0 \left\langle \frac{\partial}{\partial R_\mu} I | J \right\rangle - \varepsilon_I^0 \left\langle I | \frac{\partial}{\partial R_\mu} J \right\rangle \right) Q_\mu^\alpha, \quad (19)$$

where $|I\rangle$ is the MO state and ε_I^0 is its energy. R_μ is a Cartesian displacement coordinate for the atoms which are moved and Q_μ^α is the mass-weighted eigenvector. Note that when I is equal to J, the coupling is the deformation potential, i.e.,

$$M_{II}^\alpha = \sum_\mu \frac{\partial \varepsilon_I^0}{\partial R_\mu} Q_\mu^\alpha. \quad (20)$$

Since the term N_α does not include the factor $(f_L - f_R)$, fixing E with the Fermi level will be better than the above averaging procedure. Omitting derivatives of $T_\alpha^{\mathrm{in}}(E_F)$, etc. with respect to the bias V_b as in the case of the IETS and expanding $\Pi_{\mathrm{e\text{-}ph}:\alpha}^<(\Omega_\alpha)$ and $\Pi_{\mathrm{e\text{-}ph}:\alpha}(\Omega_\alpha)$ in the lowest order for M^α,[26] we obtain

$$N_\alpha(\Omega_\alpha) = \frac{1}{4} \frac{T_\alpha^{\mathrm{in}}(E_F) F_\alpha(V_b, T) + [T_\alpha^{\mathrm{in}(L)}(E_F) + T_\alpha^{\mathrm{in}(R)}(E_F)] \Omega_\alpha N_{\mathrm{BE}}(\Omega_\alpha, T) + 2\eta N_{\mathrm{BE}}(\Omega_\alpha, T)}{T_\alpha^{\mathrm{eh}}(E_F)\Omega_\alpha + \eta/2}, \quad (21)$$

$$\frac{dN_\alpha}{dV_b} = \frac{1}{4} \frac{T_\alpha^{\mathrm{in}}(E_F)}{T_\alpha^{\mathrm{eh}}(E_F)\Omega_\alpha + \eta/2} \frac{dF_\alpha}{dV_b}, \quad (22)$$

$$\frac{d^2N_\alpha}{dV_b^2} = \frac{1}{4} \frac{T_\alpha^{\mathrm{in}}(E_F)}{T_\alpha^{\mathrm{eh}}(E_F)\Omega_\alpha + \eta/2} \frac{d^2F_\alpha}{dV_b^2}, \quad (23)$$

where the expressions $T_\alpha^{\mathrm{eh}}(E)$ and $T_\alpha^{\mathrm{in}(L/R)}(E)$ read

$$T_\alpha^{\mathrm{in}(L/R)}(E) = \mathrm{Tr}[\mathbf{M}^\alpha \mathbf{G}_{CC}^0(E) \mathbf{\Gamma}_{L/R}(E \pm V_b/2) \mathbf{G}_{CC}^{0\dagger}(E) \mathbf{M}^\alpha \mathbf{G}_{CC}^{0\dagger}(E) \mathbf{\Gamma}_{L/R}(E \pm V_b/2) \mathbf{G}_{CC}^0(E)], \quad (24)$$

$$T_\alpha^{\mathrm{eh}}(E) = \sum_{K=L,R} \mathrm{Tr}[\mathbf{M}^\alpha \mathbf{G}_{CC}^0(E) \mathbf{\Gamma}_K(E \pm V_b/2) \mathbf{G}_{CC}^{0\dagger}(E) \mathbf{M}^\alpha\ \mathrm{Im}\ \mathbf{G}_{CC}^0(E)]. \quad (25)$$

Equations (13), (14), and (21)–(23) will be useful in calculating the IETS as well as for analyzing the change of conductance and the symmetry of IETS.

III. EFFICIENT MO APPROACH

In this section, we describe our practical NEGF-SCF algorithm, named the efficient MO approach,[13] with the improvements. Our approach aims at developing a scheme placed in a middle position between the two standard approaches, based, respectively, on the "cluster" and the "periodic slab." In the former approach, the C region is modeled by finite-size cluster (i.e., the two-dimensional periodicity of the electrodes is omitted), and the lead self-energies are parameterized by bulk data as well as long-range bulk potential. The latter approach includes the exact two-dimensional boundary condition for C; thus the system is calculated by slab or supercell model. The cluster approach is computationally efficient and enables easy modeling of low coverage and/or large E-M-E systems but it is somewhat arbitrary in defining the cluster. Furthermore, recent studies show that the extended molecule based on the cluster sometimes gives a serious fluctuation of conductance and IETS signal caused by waveguide effects.[55–58] The efficient MO approach starts from the latter periodic slab model to avoid such artificiality and inaccuracy, although it contains several aspects from the former model to maintain computational efficiency.

A. Embedding potential and correction of the density matrix

The GFMs require the Hamiltonian matrix $\mathbf{H}_{CC}$ constructed from the KS Hamiltonian, which should contain contributions from the connected deep bulk parts; thus the

best $\mathbf{H}_{CC}$ is the submatrix of the KS Hamiltonian matrix obtained from the calculation of W the system. This can contain the long-range self-consistent potential coming from L_B or R_B layers. However it is impossible to apply KS-DFT for *truly semi-infinite* W, hence one adopts $\tilde{W}$, which consists of a few buffer layers outside the C region and calculation is now possible [see Fig. 1(a)]. In the standard approach such as SMEAGOL, the L and R blocks, $\mathbf{H}_{LL/RR}$, are replaced to the bulk Hamiltonian and fixed throughout NEGF-SCF. The remaining parts in the $\mathbf{H}_{CC}$ are updated by NEGF-SCF using the result of KS-SCF for $\tilde{W}$ as an initial guess. Therefore the NEGF-SCF step is necessary even if there is not applied bias [this is sometimes called "equilibrium Green's function (EGF)-SCF"]. When one constructs the Hartree and the exchange-correlation (XC) potential in the C region by using the updated density matrix spanning the C region, long-range electrostatic potential coming from the buffer layer will be now missing. In addition, numerical continuity of $\mathbf{H}_{cL/cR}$ should be checked although the applied bias is 0 because $\mathbf{H}_{LL/RR}$ are given form bulk Hamiltonian, not the obtained self-consistent result of $\tilde{W}$. As a result one needs sufficiently large C region even if the applied bias is small. The above weakness leads to the high computational costs. Furthermore it also leads the difficulty in convergence of the NEGF-SCF (and EGF-SCF) caused by spicky density matrix when one tries to reduce the size of C region.

In our previous study, we have proposed the introduction of an embedding potential to overcome the above difficulties.[13] Here we further develop the scheme based on the embedding potential by introducing a correction term into the density matrix. The flow chart of the scheme is summarized in Fig. 1(b). The starting point is rooted in the following assumption. Suppose that one performs a standard KS-DFT calculation for the supercell $\tilde{W}$, which has a sufficient number of additional layers as buffer. If one *clip*s the Hamiltonian matrix $\mathbf{H}_{CC}[\tilde{W}]$ from the resulting KS Hamiltonian of the $\tilde{W}$ system, this $\mathbf{H}_{CC}[\tilde{W}]$ will be a good approximation for the submatrix on the C region of really semi-infinite E-M-E system W (at least at zero bias). Following Ref. 13, we introduce the notation $A[X]$ to denote that the quantity A is obtained by *clipping* the matrix obtained by an equilibrium calculation for the X system. If the above assumption is valid, then the embedding potential matrix on the C region, $\mathbf{V}_{CC}^{\mathrm{emb}}$, can be defined as

$$\mathbf{V}_{CC}^{\mathrm{emb}} = \mathbf{H}_{CC}[\tilde{W}] - (\mathbf{T}_{CC}^{\mathrm{kin}} + \mathbf{V}_{CC}^{H}\{\mathbf{D}_{CC}[\tilde{W}]\} + \mathbf{V}_{CC}^{\mathrm{XC}}\{\mathbf{D}_{CC}[\tilde{W}]\}), \tag{26}$$

where T^{kin} is the kinetic energy and $\mathbf{D}_{CC}[\tilde{W}]$ is obtained by a standard KS-DFT just like the $\mathbf{H}_{CC}[\tilde{W}]$. If the assumption is valid, we can expect that $\mathbf{D}_{CC}[\tilde{W}]$ is a good approximation for the density matrix of the C region. This embedding potential is fixed through the NEGF-SCF calculations; thus the calculation for the large $\tilde{W}$ system is only performed once. When one performs NEGF-SCF, the electrostatic potentials (and continuity) due to existence of L_B and R_B parts are partially incorporated without explicit consideration of the buffer layers. These procedures lead another small difference from the standard scheme. In our scheme, the L and R blocks are also fixed through NEGF-SCF but no replacement to the bulk terms. To maintain consistency between our scheme and the standard NEGF-SCF scheme, we need to enforce the match of the density matrices between the EGF-SCF for the C region and the clipped matrix resulting from the equilibrium (i.e., KS-SCF) calculation for the $\tilde{W}$. Then we can introduce a correction factor for the density matrix

$$\Delta\mathbf{D}_{CC} = \mathbf{D}_{CC}[\tilde{W}] + \frac{i}{\pi}\int dE\mathbf{G}_{CC}^{0<}(E)|_{V_b=0}. \tag{27}$$

The EGF-SCF procedure combined with definition of a correction term is schematically given in Fig. 1(b). In the general NEG-SCF step, the Hartree and XC potential terms are updated by the corrected density matrix as

$$\mathbf{D}_{CC} = \frac{-i}{\pi}\int dE\mathbf{G}_{CC}^{0<}(E) + \Delta\mathbf{D}_{CC}. \tag{28}$$

Indeed, the factor $\Delta\mathbf{D}_{CC}$ should be close to 0 (if this is not the case, our assumption will break down). However, *ab initio* calculations of $\mathbf{G}_{CC}^{0}(E)$ sometimes provide numerical instability for the sampled energy grid. As an example, when the electrodes have a dense and complex structure, a very large C region is required to eliminate such an instability.[11,59] Similarly the existence of a few strongly localized states on the surfaces or of van Hove's singularity leads to similar instabilities.[60,61] Therefore, $\Delta\mathbf{D}_{CC}$ is useful for stable convergence of the NEGF-SCF without increasing the sample energy grids for the energy integral, while maintaining consistency with the embedding potential scheme. We emphasize that the above scheme can describe the response of the given E-M-E system to the applied voltage at the same level as a standard NEGF based on the "periodic slab" approach, although our scheme has the flexibility of a practical combination of approximations. For instance, we can use a KS-DFT result converged with sufficient k sampling to define $\mathbf{H}_{CC}[\tilde{W}]$ and $\mathbf{V}_{CC}^{\mathrm{emb}}$ at the Γ point and $\Delta\mathbf{D}_{CC}$. Then the NEGF-SCF calculation for nonzero bias can be performed at the Γ point only. In this case, the system is described with high accuracy by means of fine k-point sampling, but the response to the applied bias is reduced to a Γ-point calculation.

B. Expansion of the MO basis and restricted MO space

In order to perform practical NEGF-SCF steps, we employ a perturbation expansion of the Green's functions (PT-GFs) in the MO basis. This is obtained by diagonalizing the KS Hamiltonian spanning the C region. The PT-GF matrix $\mathbf{G}_{CC}^{\mathrm{PT}}$ can be represented by the following diagonal matrix:

$$\mathbf{G}_{CC}^{\mathrm{PT}}(E) = \mathrm{diag}\left[\left\{E - \varepsilon_I^0 - \frac{i}{2}(\Gamma_{L,I}(E + V_b/2) + \Gamma_{R,I}(E - V_b/2))\right\}^{-1}\right], \tag{29}$$

where the term ε_I^0 is the energy of the Ith MO. From the KKB equation, the lesser PT-GF, $\mathbf{G}_{CC}^{\mathrm{PT}<}(E)$, can also be writ-

ten as a diagonal matrix. In each NEGF-SCF step, the density matrix is constructed by simply calculating the *electron-occupation number* of each MO I,

$$d_I = \frac{-i}{\pi}\int dE \mathbf{G}^{\mathrm{PT}<}_{CC}(E). \tag{30}$$

Here we recall that we incorporate the factor 2 for spin degeneracy and that d_I is transformed back to the AO representation when updating the Hamiltonian. One of the great advantages of using PT-GFs in the MO basis is that the numerical evaluation of d_I is much easier and faster than calculating $\mathbf{D}_{CC}$ by using the full $\mathbf{G}^{0<}_{CC}$ density matrix directly. Furthermore, one can introduce an approximation by replacing E with E_F or with ε^0_I in $\Gamma_{L/R}(E)$. If one uses one of the above approximations, the integral in Eq. (30) is further simplified and a quite accurate evaluation is possible by using the polynomial expansion technique without the need for a large number of energy grid points.[62]

The use of the PT-GFMs is restricted only to the NEGF-SCF step in our algorithm; the final calculations to obtain transport properties such as current and IETS are performed using the full GFMs after the convergence of the NEGF-SCF is achieved. Since our efficient MO approach contains the scheme for the corrected density matrix described in Sec. III A, the error caused by the use of PT-GFs instead of the full Green's functions is restricted only to the response of the central region to the applied bias (charge transfer, net charge, polarization). In our previous study, we analyzed the validity of the perturbation expansion in the NEGF-SCF step and the use of the embedding potential for the BDT/Au(111) system and compared the obtained induced charge with the results by the standard use of full GFM as well as the electric field induced by the applied.[13] We found that that the use of Eq. (29) is a good first approximation to estimate the change of charge by the applied bias and also the condition that the off-diagonal element of $\mathbf{\Gamma}_{L/R}$ is usually much smaller than the diagonal element is satisfied. Recently, we have applied our scheme to the calculation of an Au atomic wire attached to Au electrodes, i.e., to a highly conductive system. In Ref. 58, we checked the validity of the use of the embedding potential and PT-GF for NEGF-SCF and also found that the transmission coefficients and the effects due to the applied bias are in reasonably good agreement, just as in the BDT case. We have checked the matrix elements in the MO basis for the Au wire system. Typically, the ratio of the off-diagonal to the diagonal elements, Γ_{IJ}/Γ_{II}, was lower than 0.3, a value only slightly larger than that observed for the case of BDT (typically $\Gamma_{IJ}/\Gamma_{II} \approx 0.1$). Hence, we conclude that the condition that the off-diagonal element of $\mathbf{\Gamma}_{L/R}$ is usually much smaller than the diagonal element is satisfied for both the BDT molecule and the Au wire. Note that the condition $|\Gamma_{IJ}/\Gamma_{II}| \ll 1$ does not justify the use of MOs as the zeroth-order "eigenstates" in the perturbation theory.

However, the use of PT-GFs (and related matrices) seems to be valid even if the perturbation theory for the eigenstate is not suitable because the GFMs are the inverse of the (effective) Hamiltonian as given in Eq. (2). The omission of the off-diagonal elements of the effective Hamiltonian expanded by the same MOs does not produce serious changes to its inverse. This is in general true as long as the diagonal elements are larger than the off-diagonal ones. In this case, the diagonal elements in the lesser GF consist of the factor of $O(\Gamma_{II}/\Gamma_{II} \sim 1)$ but the factor in the off-diagonal elements is $O(\Gamma_{IJ}/\Gamma_{II})$. Thus the use of Eq. (29) in the NEGF-SCF step can be a good first approximation when $|\Gamma_{IJ}/\Gamma_{II}| \ll 1$. We remind the reader that the response (charge donation/back donation, etc.) caused by the connection to the electrodes (sometimes a strong interaction) is incorporated in the EGF-SCF stage, i.e., it is free from the use of PT-GFs. Again, we emphasize that the use of PT-GFs is only for estimating the change in the density matrix caused by the applied bias.

To make the NEGF-SCF step even more efficient, we have proposed a "restricted MO space" scheme and we have applied it to several systems. Since we adopt this idea in the present calculations, here we briefly provide an outline of the method. Further details are given in Ref. 13. The concept of the restricted MO space is similar to the scheme of the complete active space (CAS) (Ref. 63) or fully optimized reaction space (FORS) (Ref. 64) in quantum chemistry. The central goal of the NEGF-SCF step is to determine the occupation number, d_I, as shown in Eq. (30). On one hand, if the MO energy is much lower than the Fermi energy, the occupation number can always be fixed to 1; thus these MOs are electrically "inactive"(filled at any relevant bias). On the other hand, MOs whose energies are much higher than the Fermi level will always be empty, i.e., their occupation number can always be fixed to 0 and they can be regarded as "virtual" MOs. Therefore, the occupation numbers should be determined by the KKB equation as nonequilibrium quantities only for the "active" MOs, whose energy is within the bias window or around the Fermi level for the zero-bias limit. These form the restricted MO space as a small part of the entire MO space. The size of the restricted MO space can be fixed by the bias range for the system of interest. Usually, the applied bias is a few volts against an electrode bandwidth of a few tens of volts, hence the restricted MO space is smaller than 10% of the entire MO space. Note that the fixed occupation in the present NEGF-SCF scheme is imposed only to the inactive and virtual MOs. However orbital relaxation is allowed for all MOs since the Hamiltonian is constructed from the new density matrix.

C. Accurate $O(N)$ algorithm for a lead self-energy matrix

For quantitative calculations of nanodevices it is important to model the electrodes as well as the contacts. There are several methods for constructing the lead self-energy matrices by *ab initio* calculations within a mean-field approximation such as DFT. In the present study, we adopt the tight-binding-layer (TBL) scheme combined with the decimation procedure.[14,59,61] The TBL scheme can incorporate exact semi-infinite contacts, which should include both Bloch and evanescent states, and the numerical singularities are eliminated by decimation. Since the TBL Hamiltonian is constructed from the bulk KS-DFT Hamiltonian, the resulting $\mathbf{\Sigma}_{L/R}$ terms are estimated at the same level of accuracy as $\mathbf{H}_{CC}$. The TBL scheme requires solving a general eigenvalue

problem; thus the computational cost is $O(N^3)$. However, the electrodes sometimes have a much more regular periodic structure, consisting of the $N_{\mathrm{cell}} \times N_{\mathrm{cell}}$ primitive cells, than the contact region. In this case, one can calculate the self-energy matrices at an $O(N)$ computational cost.

Our basic strategy takes from the scheme of Damle *et al.*,[65] i.e., instead of a direct calculation of the self-energy matrix of the total $N_{\mathrm{cell}} \times N_{\mathrm{cell}}$ electrode, calculations of a self-energy matrix $\mathbf{\Sigma}^0_{L/R}(E:\vec{k}_{\|})$ for one primitive unit cell with sufficient $\vec{k}_{\|}$ point sampling are performed instead. These are then extended to the total L/R regions by making Fourier copies of the primitive cell

$$[\Sigma_{L/R}(E)]_{\mu'\nu} = \sum_{\vec{k}_{\|}} [\Sigma^0_{L/R}(E:\vec{k}_{\|})]_{\mu\nu} \exp[-i\vec{k}_{\|}(\vec{R}'_{\mu} - \vec{R}_{\nu})], \tag{31}$$

where μ' is the AO for the atom in the electrode of interest, but μ is for the equivalent atom in the primitive unit cell. The vector $\vec{R}'_{\mu}$ corresponds to the position vector. Note that $\vec{k}_{\|}$ is the wave vector parallel to the surface (in the plane orthogonal to the transport). Since we can construct total self-energy matrices by solving eigenvalue problems only for the one primitive unit cell, the use of Eq. (31) provides an $O(N)$ algorithm. As a test, we have calculated the transmission coefficient of the Au wire formed by six atoms attached to the (001) surface in the 0 bias limit. These results have been then compared to those obtained with a standard (direct) calculation of $\mathbf{\Sigma}_{L/R}$, performed with the SMEAGOL program.[14,65,66] For simplicity, we adopt Γ-point values for both NEGF calculations and the electrodes have 3×3 structure; thus N_{cell} is set to 3. In order to reproduce the TBL Hamiltonian of 3×3 bulk structure, we took $15 \times 15 \times 20$ for $\vec{k}$-point sampling, we calculate the TBL Hamiltonian of the primitive unit cells of the left-hand side and right-hand side leads, then construct $\mathbf{\Sigma}^0_{L/R}(E:\vec{k}_{\|})$. In Fig. 2, the transmission coefficients as a function of energy are given as well as a schematic picture of the C region. The curve calculated by the direct evaluation of $\mathbf{\Sigma}_{L/R}$ is almost 1 and constant over the energy region close to the Fermi level. This is the typical behavior of an Au atomic wire and it is consistent with previous theoretical and experimental studies. In contrast, the result obtained by the simple use of Eq. (31) shows unphysical oscillations and could not reproduce the constant transmission coefficient. Failures of the simple Damle scheme are caused by different boundary conditions enforced on $\mathbf{H}_{CC}$ (periodic for the direction parallel to the surface) and $\mathbf{\Sigma}_{L/R}$ because summing all $\vec{k}_{\|}$ in Eq. (31) is a Fourier transformation but does not necessarily satisfy the same boundary condition. Even if the set of $\vec{k}_{\|}$ vectors in Eq. (31) is selected as the same set used for constructing the bulk Hamiltonian for the primitive unit cell, the above mismatch is not eliminated. Physically, this is a waveguide effect, i.e., it originates from the quantum interference of the electronic transverse modes because the C region is a two-dimensional (periodic) system but $\mathbf{\Sigma}_{L/R}$ is a (quasi) one-dimensional system.

In order to eliminate the nonphysical waveguide effect, we introduce the following condition over $\vec{k}_{\|}$ in Eq. (31):

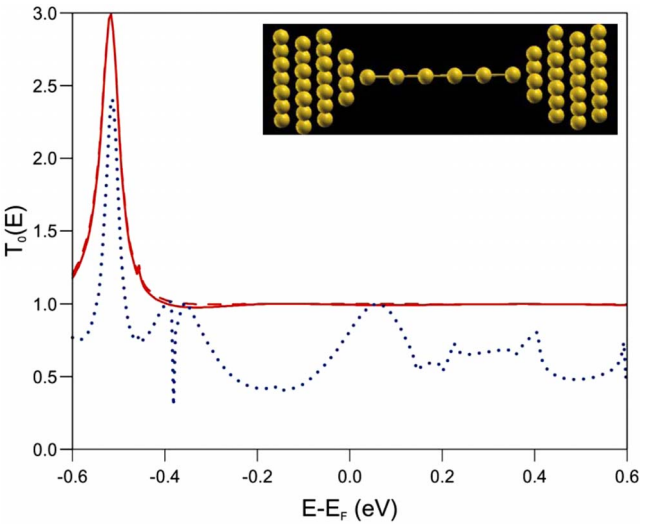

FIG. 2. (Color online) The transmission coefficient, $T_0(E)$, for the Au wire in the Au(001) systems. The wire contains six Au atoms attached on the 2×2 plateau with 3×3 electrodes, which is displayed in the inset. $T_0(E)$ is plotted as a function of electron energy. The red (dark gray) solid line and (completely overlapped) dotted line are the results by the standard method and by our $O(N)$ scheme, respectively. The blue (light gray) dotted line represents the result by the $O(N)$ method *without* the condition given in Eq. (32).

$$\vec{k}_{\|} \cdot (N_{\mathrm{cell}}\vec{t}) = 2n\pi, \tag{32}$$

where $\vec{t}$ is a translational vector of the primitive unit cell of the electrode relating to $\vec{k}_{\|}$ and n is an integer. The above condition enforces the same boundary condition to the self-energy matrices with two-dimensional Bloch waves (in the present case, Γ point approximation) used to expand the C region. The transmission coefficient calculated using Eqs. (31) and (32) is shown in Fig. 2, where one can find a perfect agreement with the result obtained by calculating $\mathbf{\Sigma}_{L/R}$ directly. Our $O(N)$ scheme can be summarized as follows.

(1) Set the primitive unit cells, which are the minimum units for the left-hand side and right-hand side electrodes of the system under investigation, and define the sets of the related translational vector $\vec{t}$ and the number of the contained primitive unit cells N_{cell}.

(2) Calculate the TBL Hamiltonian matrix of the primitive unit cell with a sufficient $\vec{k}$-point sampling.

(3) Construct the self-energies $\mathbf{\Sigma}^0_{L/R}(E:\vec{k}_{\|})$ by using the above TBL Hamiltonian, where $\vec{k}_{\|}$ should satisfy the condition of Eq. (32).

(4) Calculate the required self-energies $\mathbf{\Sigma}_{L/R}(E)$ defined on the L/R region by extending the primitive cell as indicated in Eq. (31) with use of the above selected $\vec{k}_{\|}$-point sampling.

Although we have adopted the Γ-point approximation for the C region in the present example, our method can be extended to more general cases by estimating the self-energies for supercells (larger than the L/R regions) by replacing $\vec{t}$ with the translational vector of the defined supercell. Then one can evaluate the self-energy matrices

describing the supercell by using $\vec{k}_{\parallel}$ points together with the condition of Eq. (32).

IV. APPLICATION: THE "0.5 RULE" AND SYMMETRY

In this section, we apply our method to an Au atomic wire and a BDT molecule both attached to Au electrodes. One of our focuses is the comparison of the inelastic transport properties in the "low-conductance regime" with that in the "high-conductance regime;" in particular, we will compare the changes in conductance and the shape of IETS of realistic systems. In addition, we have an interest in the molecular (contact) symmetry and the IETS signal. Though a single and free BDT molecule has D_{2h} symmetry, the moiety constructed by BDT and Au electrodes generally does not have D_{2h} structure. This is inconvenient when analyzing the relation between symmetry and IETS activity since the same analysis carried out by separating the BDT from coupled Au electrodes is unclear. However if one adopts (001) structure for Au electrodes, the moiety (i.e., C region) can maintain high symmetry (D_{2h} for zero bias, C_{2v} for nonzero bias); thus this system is a good prototype for analyzing the properties of the IETS in molecular junctions. For both systems, we have checked the validity of the presented NEGF scheme by comparing some results such as the transmission coefficients and the self-consistent mean-filed potentials with results obtained by using SMEAGOL as well as with previously published studies.

For all the calculations, we adopted the Perdew-Burke-Ernzerhof (PBE) XC functional.[67] The basis set used for all the atoms is a pseudoatomic orbital (PAO)-type at the single zeta polarized (SZP) level, and Troullier-Martins norm-conserving pseudopotentials are used for the core electrons.[68] The KS-DFT sections are performed with SIESTA,[69] and the calculations of electron-phonon coupling, NEGF-SCF, and related properties are obtained by using our own program, which extends over SIESTA.

A. Linear Au atomic wire

The calculated Au atomic wire is displayed in the inset of Fig. 3(a). We consider a linear Au wire connected to Au(001) $4\sqrt{2}\times 4\sqrt{2}$ electrodes and only each top layer has $2\sqrt{2}\times 2\sqrt{2}$. The wire part consists of four Au atoms. The C region includes the wire and four monoatomic layers placed at both the left- and the right-hand sides of the wire. Two-dimensional periodic boundary conditions are imposed in the direction orthogonal to the transport. The two outermost layers at each side of the C region are taken as L and R regions. We have fixed the distance between the second layers at each side at 16.88 Å and set the lattice constant of Au to the experimental value of 4.08 Å. Only parts of the two top layers and wire are relaxed so that the vibrational box contains only 12 atoms.

In order to construct the embedding potential and the correction factor for the density matrix, we formed the $\tilde{W}$ by adding three and two layers, respectively, outside the L and R regions as buffer. The phonon modes in the wire are calculated by constructing the Hessian matrix. This is obtained from total-energy calculations of the $\tilde{W}$ by moving the atoms in the vibrational box. The e-ph coupling is also obtained by numerical differentiation of the same KS-DFT procedure, where only a part of the C region is *clipped* just as the Hamiltonian as shown in Sec. III A. All of the above KS-DFT calculations are performed initially for a sufficient $\vec{k}$-point sampling (in the present case $5\times 5\times 1$). Then the required matrices for the NEGF calculations are constructed at the Γ point using the converged results. In the NEGF-DFT,

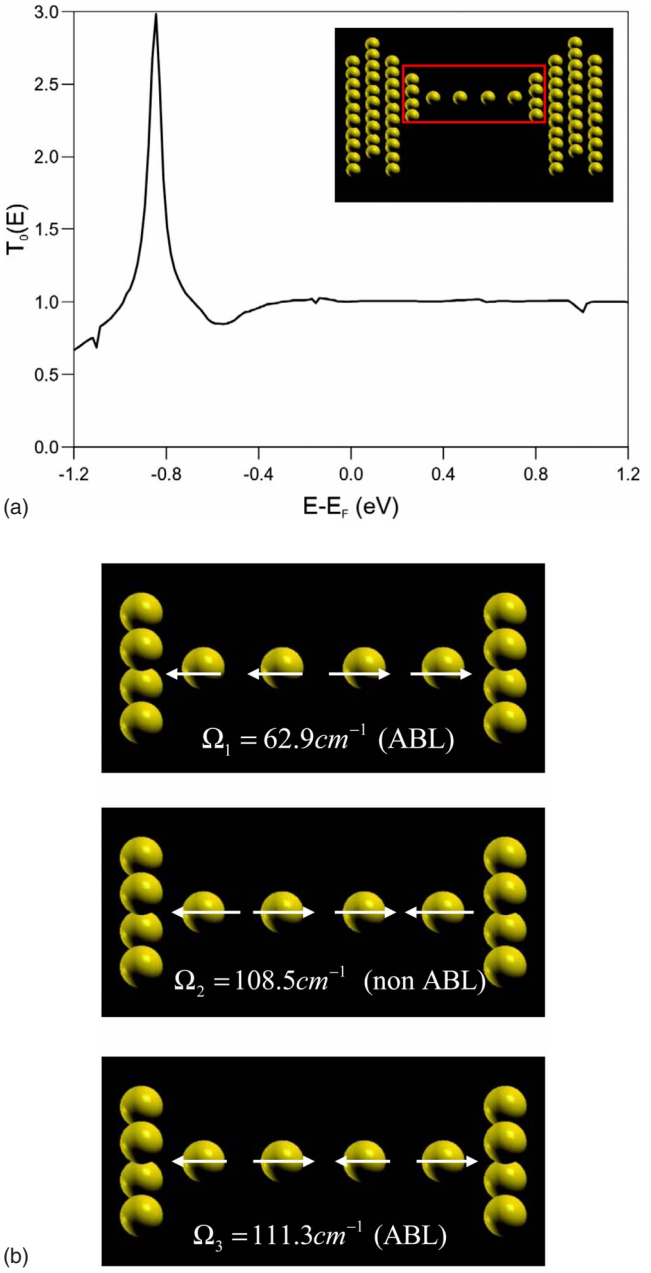

FIG. 3. (Color online) (a) The transmission coefficient, $T_0(E)$, for the four Au atomic wire. The black solid line is $T_0(E)$ plotted as a function of electron energy. The chain is attached on the $2\sqrt{2}\times 2\sqrt{2}$ plateau with $4\sqrt{2}\times 4\sqrt{2}$ electrodes and the C region is shown in the inset. The vibrational box is marked by a red (light gray) solid line. (b) The eigenvectors for the three longitudinal modes in the wire.

the estimation of the conductance and the IETS is carried out at the Γ point only. Since the electrodes have primitive unit cells of $\sqrt{2}\times\sqrt{2}$ structure, our $O(N)$ scheme was performed by setting N_{cell} to 4.

Our main focus in the present inelastic calculation is that of obtaining the IETS, therefore it is sufficient to consider the low-bias regime only, and we set max/min bias to ± 0.3 V. In order to obtain the restricted MO space, we have selected the active MOs that cover the MO energies in the range $[E_F-0.5, E_F+0.5]$ eV, where the MO energies are assigned by the zero-bias limit. We found that the size of the restricted MO is sufficient to get the converged results for NEGF-SCF in the present bias range. The calculated transmission coefficient as a function of electron energy is presented in Fig. 3(a). One can observe two main features. First the value of T_0 is almost 1 over a wide energy range around the Fermi energy, in particular above E_F. Second there is a peak much larger than 1 at around $E-E_F\sim 1.0$ eV. These features agree well with the previous theoretical results obtained with SMEAGOL with extensive $\vec{k}_{\parallel}$-point sampling.[14]

From the Hessian, we have calculated seven phonon modes related to the internal modes in the wire. Since the transverse modes are less important than the longitudinal ones, we focus only on the three longitudinal modes, $\{\Omega_\alpha\}_{\alpha=1,2,3}$, with wave numbers of 62.9, 108.5, and 111.3 cm^{-1}, respectively. In Fig. 3(b), the three eigenvectors are shown. Modes Ω_1 and Ω_3 are the alternate bond length (ABL) modes, and the second mode Ω_2 is a non-ABL mode. The change of conductance ΔG and IETS $\frac{dG}{dV_b}$ are calculated in several different situations by varying the temperature T (5, 15, and 30 K) and broadening parameter η (damp/undamped limit, 0.01, 0.05, and 0.1 meV). In Fig. 4(a), the conductance change due to e-ph interaction, defined as $\frac{d(\delta I^{\mathrm{el}}+I^{\mathrm{inel}})}{dV_b}$, and the IETS, $\frac{dG}{dV_b}$, are given as functions of the bias for a fixed temperature of 5 K. The conductance change decreases and the IETS displays a dip for all of the modes. This means that the 0.5 rule is actually satisfied. The values of ΔG for each mode are also shown in the inset of Fig. 4(b) for the undamped limit. The contribution of the non-ABL mode Ω_2 is much smaller than that arising from the ABL modes and it is almost inactive in the IETS. The most active mode is the highest ABL, which is 3–4 times larger that all the other ABL modes at all η values considered, as shown in Fig. 4(c). The IETS activity of the ABL modes and the fact that the largest intensity comes from the highest among the ABL modes have been demonstrated in other studies of linear Au wires even though the length of wire was different in every study.[2,23,25,26] The intensities of IETS decrease with increasing η, but the relative intensities of each mode change little.

In order to proceed with our analysis, we show the scaled transmission functions, $\bar{T}_\alpha^{\mathrm{ec/ecSym/in}}$, as a function of V_b in Fig. 5. From Eq. (14), the IET is determined by $\bar{T}_\alpha^{\mathrm{ec}}$ and $\bar{T}_\alpha^{\mathrm{in}}$ in the undamped limit, but they are dominated by $\bar{T}_\alpha^{\mathrm{ecSym}}$ and $\bar{T}_\alpha^{\mathrm{in}}$ in the damped one. Figure 5 shows that the terms $\bar{T}_\alpha^{\mathrm{ec}}$ and $\bar{T}_\alpha^{\mathrm{ecSym}}$ have almost equal negative values and their absolute values are more than ten times larger than that of $\bar{T}_\alpha^{\mathrm{in}}$ (we recall that $\bar{T}_\alpha^{\mathrm{in}}$ is always positive). The dependence on the bias is quite weak and in fact negligible in the present case. Therefore, the IETS always shows dips, and the relative intensities for each mode are unchanged when going from the damped to the undamped limit.

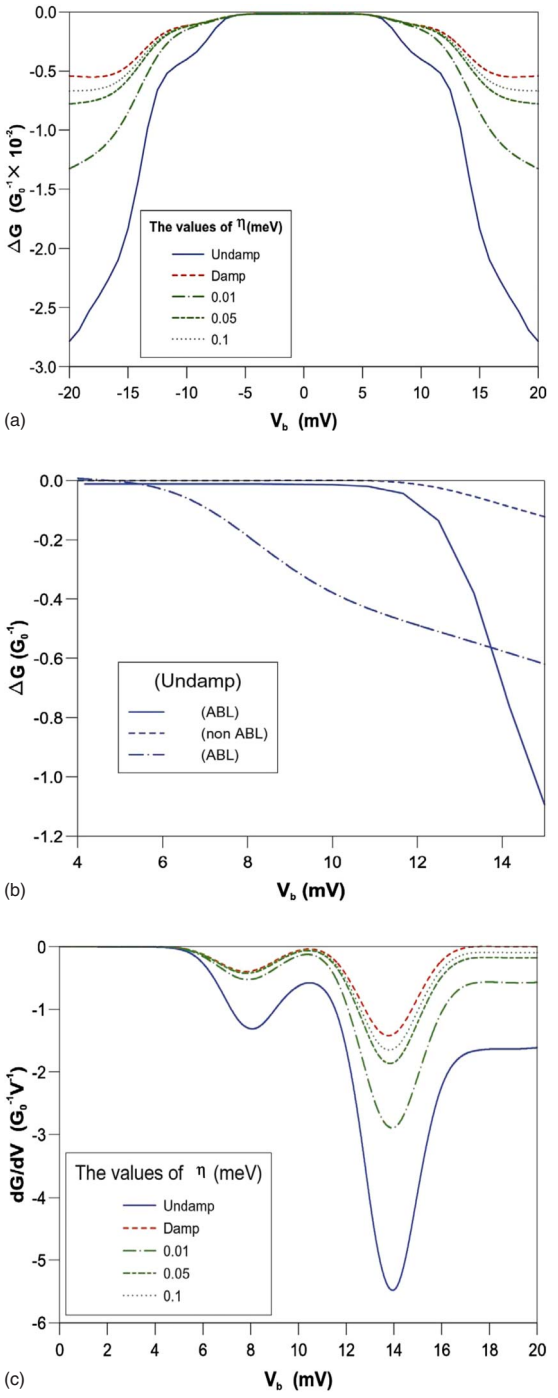

FIG. 4. (Color online) (a) The change in conductance, ΔG, in the undamped limit for the Au wire system given in Fig. 2. The included phonons are three internal longitudinal modes, which consist of two ABL modes and one non-ABL. (See the text.) The temperature is fixed at 5 K, and the parameter η is taken to equal 0.01, 0.05, and 0.1 meV, and damped/undamped limiting cases. In (b), the conductance drops related to each of the three modes are shown separately only for the undamped limit. (c) The IETS signal.

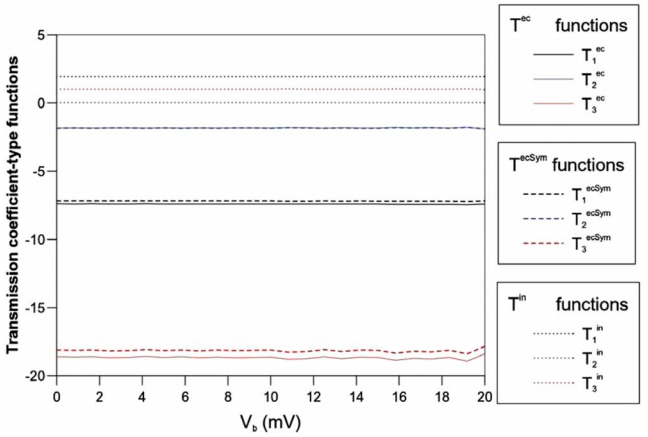

FIG. 5. (Color online) A plot of transmission coefficient-type functions, $\bar{T}_{\alpha}^{\mathrm{ec/scSym,in}}$, as functions of the bias for the Au wire system. The mode index α relates to the mode Ω_{α} in the Au wire as given in the text. The values are scaled by $\bar{T}_3^{\mathrm{in}}$ for 0 bias, i.e., $\bar{T}_3^{\mathrm{in}}$ in the 0 bias calculation is set to 1. The solid, dashed, and dotted lines represent $\bar{T}^{\mathrm{ec}}$, $\bar{T}^{\mathrm{ecSym}}$, and $\bar{T}^{\mathrm{in}}$, respectively. The sets of black, blue (dark gray), and red (light gray) lines relate to the modes Ω_1, Ω_2, and Ω_3.

The fact that $\bar{T}_{\alpha}^{\mathrm{ec}}$ and $\bar{T}_{\alpha}^{\mathrm{ecSym}}$ have almost the same values for any α can be explained by using the "single (resonant)-level model" just like the 0.5 rule since the Au wire has a single transmission eigenchannel related to the Au 6*s* electron.[2,20] By considering Eqs. (16) and (17), one can find out that the difference between $\bar{T}_{\alpha}^{\mathrm{ec}}$ and $\bar{T}_{\alpha}^{\mathrm{ecSym}}$ is proportional to the real part of the Green's function in this single-level case. For simplicity, we set the energy E to E_F (this will satisfied in our analysis of the low-bias regime) and it can be represented as

$$\mathrm{Re}[G(E_F)] = \frac{1}{\Delta E + \Gamma^2/\Delta E}, \tag{33}$$

where ΔE is the energy gap between the resonant level and the Fermi level and Γ is the coupling for both electrodes. Since the gap is close to 0 and the coupling is sufficiently large for an Au (metallic) wire, one can expect $\mathrm{Re}[G(E)]$ to be close to 0, i.e., $\bar{T}_{\alpha}^{\mathrm{ec}} \approx \bar{T}_{\alpha}^{\mathrm{ecSym}}$ for all modes.

Next we analyze the temperature dependence of the IETS signal. Figure 6 shows the IETS for the damped limit. By increasing the temperature through the values 5, 15, and 30 K, the dips become broader. This is consistent with the behavior of the second derivatives of $F_{\alpha}(V_b,T)$, which are independent of details of the electronic structure. It is interesting that the dip of the first ABL mode is hindered at $T \approx 15$ K by the long tail of the broad dip relating to the highest (most active) ABL mode. This means that some active modes do not appear in the IETS when (a) the system has strongly active modes, (b) the experimental temperature is slightly higher than the mode energy, or (c) the internal modes are strongly coupled with the bath.

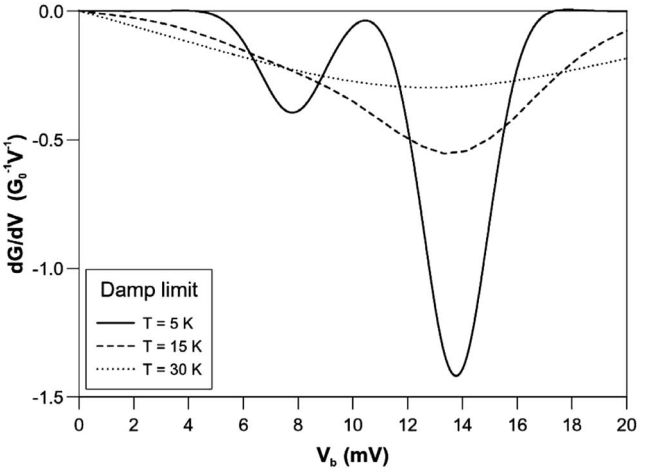

FIG. 6. The temperature dependence of the IETS signals in the damped limit for the Au wire system. The black solid, dashed, and dotted lines represent the IETS signals for temperatures of 5, 15, and 30 K, respectively.

B. BDT in D_{2h} symmetry

The next example is that of the BDT molecule attached to the hollow site of Au(001) surfaces in the $4\sqrt{2}\times 4\sqrt{2}$ structure. A picture of the *C* region and vibrational box is given in Fig. 7(a). The structure maintains D_{2h} symmetry not only when the BDT molecule is considered but also in the entire *C* region. Strictly speaking, the symmetry reduces to C_{2v} when the bias is applied, however we will keep using the irreducible representations of the D_{2h} point group. Furthermore, the D_{2h} symmetry can be relaxed to the lower (but more general) symmetry C_{2h}. For later use, we survey the symmetry operations that define the point groups. Let us define the *xyz* coordinates as follows. The transport direction is set along the *z* axis and the BDT molecular plane lies in the *yz* plane. Then we can define the D_{2h} symmetry elements, which consist of three C_2 axes, three $\sigma_h(x,y,z)$ planes, the *x*, *y*, and *z* axes, and the *yz*, *zx*, and *xy* planes, respectively. If a bias is applied, the symmetry is reduced to C_{2v}, where the C_2 axis is the *z* axis and the two σ_v planes are the *yz* and *zx* planes. In contrast, if the electrodes are not $n\sqrt{2}\times n\sqrt{2}$ or not (001) surfaces, the symmetry reduces to C_{2h}. In this case, the C_2 axis is the *x* axis and σ_h is the *yz* plane. The relations between the sets of irreducible representations in each of the point groups are summarized in Table I. The procedures for constructing the embedding potential, the self-energies, the Hessian, and the e-ph coupling matrix are the same as in the case of the Au atomic wire. The calculated transmission coefficient is given in Fig. 7(a) and it reproduces the results of the previous calculations obtained with SMEAGOL, such as the order of magnitude of $T_0(E_F)$ ($\sim$0.05) and the broad peak below the Fermi level.[55,70–72] For the present BDT/Au(001) system, we modeled the restricted MO space for the NEGF-SCF as the active MOs that cover the MO energies between $(E_F-0.8)$ and $(E_F+0.8)$ eV. The resulting restricted MO space provided the converged results within the range of bias $V_b \in [-0.5, 0.5]$ eV.

By normal-mode analysis of the vibrational box, we could assign the 30 internal modes corresponding to the BDT mol-

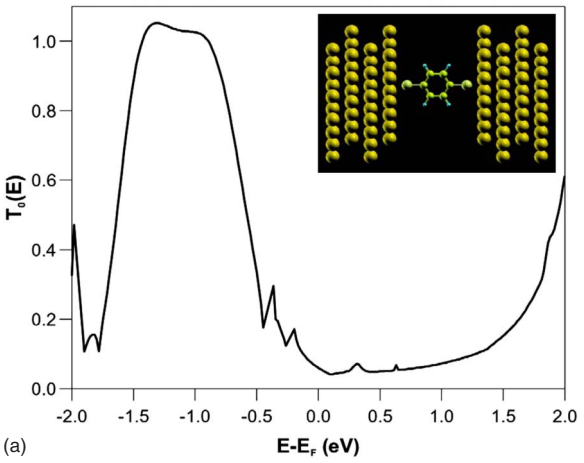

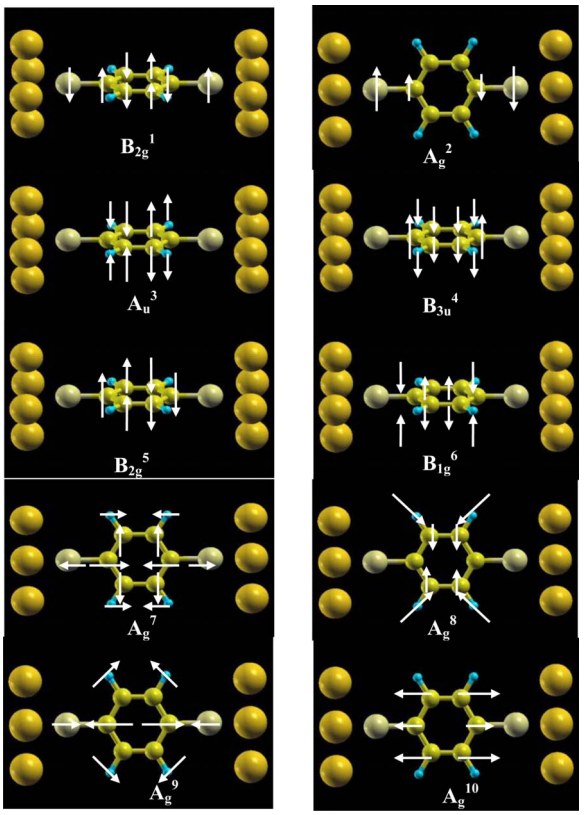

FIG. 7. (Color online) (a) The transmission coefficient, $T_0(E)$, for BDT on the Au(001) electrodes. $T_0(E)$ is plotted as a function of electron energy. The BDT molecule is attached on the hollow site of the Au(001) surface, which has the $4\sqrt{2}\times 4\sqrt{2}$ structure. The C region is shown in the inset. (b) The eigenvectors of the ten selected active modes for the IETS, where each mode is assignable to the free BDT molecular internal modes. The labels represent the related irreducible representation in the D_{2h} point group and the numbering of the modes. (See the text.)

ecule. We concentrated only on the low internal modes, whose frequencies are within 0.2 eV, and found ten clearly active modes by checking the transmission functions. A list of all of the modes, $\{\Omega_\alpha\}_{\alpha=1-10}$, is given with their irreducible representation labels in Table I, and the related eigenvectors

TABLE I. The ten selected active modes for the IETS of the BDT/Au system. The mode labels represent the related irreducible representations (irreps) in the D_{2h} point group and numbering. (See the text.) The value Ω is the wave number (in cm^{-1}). The relationships to the irreps of the lower symmetry C_{2v} and C_{2h} groups are also given.

Mode	Ω (cm^{-1})	C_{2v} irreps.	C_{2h} irreps.
B_{2g}^1	195.2	B_1	B_g
A_G^2	330.9	A_1	A_g
A_u^3	333.7	A_2	A_u
B_{3u}^4	360.7	B_1	A_u
B_{2g}^5	543.6	B_1	B_g
B_{1g}^6	668.1	A_2	B_g
A_g^7	682.5	A_1	A_g
A_g^8	958.7	A_1	A_g
A_g^9	1040.9	A_1	A_g
A_g^{10}	1546.7	A_1	A_g

are shown in Fig. 7(b). For convenience, we denote a mode as A_g^2, etc., where "A_g" is the label of an irreducible representation in D_{2h}, and the index "2" means that α is 2, i.e., it is the second of the selected ten modes. We found that the values of Ω_α are renormalized by the existence of the electrodes, but the eigenvectors have a clear one-to-one correspondence to the eigenvectors of the free BDT molecule. The calculated total IETS is shown in Fig. 8(a) for both the damped and the undamped limits at $T=5$ K. First, we found five totally symmetric modes (A_g) in the considered energy range, and all of these modes are active for the IETS. The most active among the ten active is the totally symmetric stretching mode, A_g^{10}, and the tendency of the relative intensities of the remaining A_g modes agrees well with the results obtained by Gagliardi *et al.*[41] and by Troisi and Ratner,[47] although their formulations of IETS are restricted to damped limit case with omitting elastic correction terms. In their calculations, all values of the frequencies (particularly for the asymmetric modes) are slightly different from ours because of the difference choice of adopted C region when modeling the E-M-E system. However, the eigenvectors are assignable to the modes of the isolated BDT molecule in both the previous study and our study; thus it is meaningful to compare symmetry properties for these studies in the damped limit case.

In the MO basis, the e-ph coupling M^α has nonzero diagonal elements only for the A_g modes. Hence, the deformation potential, which is defined as the derivative of the MO energy, will dominate the IETS intensities. In contrast, the symmetry properties for the asymmetric modes are much more complex to analyze because only the coupling through the different MOs is dominant. The ten most active modes obtained by Gagliardi *et al.*[41] consist of five A_g, two B_{2g}, one B_{3u}, one B_{1g}, and one A_u modes. In the present study, the B_{1g} mode is more active than the B_{3u} in their result, but the two resulting sets of active modes agree well in the damped limit. Since the B_{1g} and A_u modes belong to the same A_2 irreduc-

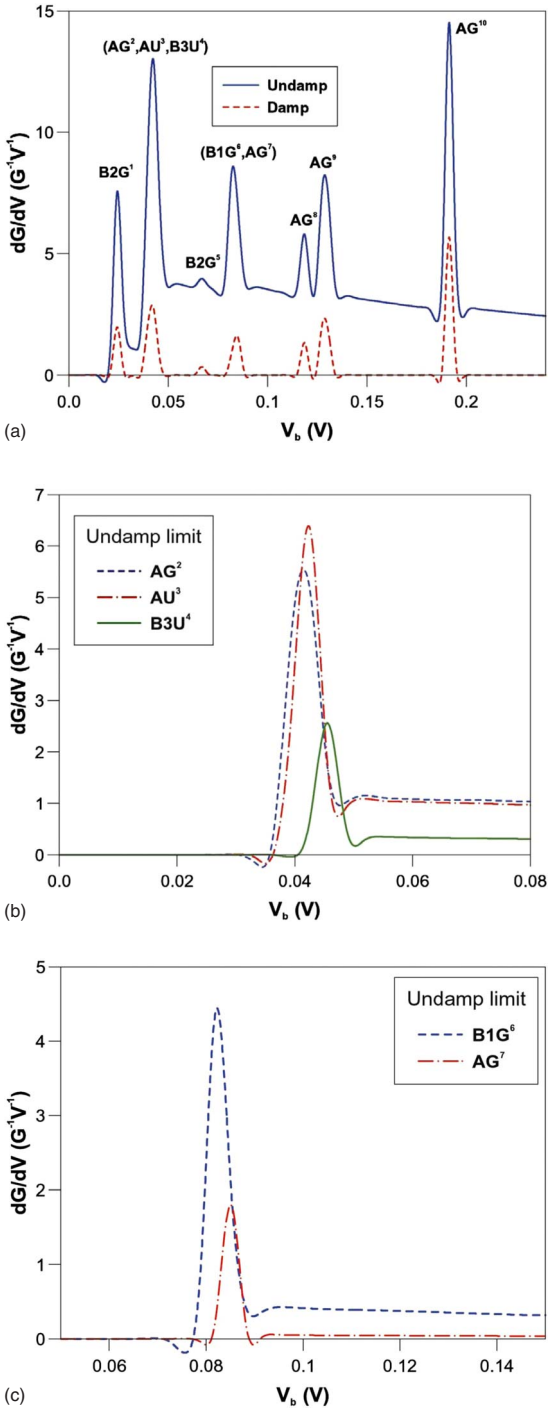

FIG. 8. (Color online) (a) The IETS signals for the BDT/Au system. The dashed red (gray) line represents the IETS in the damped limit and the solid blue (gray) line is for the undamped limit. The temperature is fixed at 5 K. Each mode relating to the peak positions of the signals is also shown. The detailed structures of the moiety, which consist of several peaks corresponding to each mode, are shown for the undamped limit in (b) and (c).

ible representation of the C_{2v} point group, related pathways may be mixed when bias is applied in our model. In the energy range below 0.1 eV, the highest peak of IETS is for the B_{2g} modes, whose intensities are comparable to the IETS of the A_g modes. This feature agrees with the result of Troisi and Ratner[47] but not with those of Ref. 41. Furthermore, the active asymmetric modes are only the out-of-plane modes; hence the propensity rule proposed in Ref. 47 is satisfied here in our damped limit calculation. However, the details of the relative IETS intensity of each mode seem to be quite sensitive to the degree of damping used in the calculations except for the A_g modes. It is then difficult to formulate stricter selection rules for higher symmetry such as D_{2h} by comparing our data or previous studies.

TABLE II. The transmission functions, T^{ec}, T^{ecSym}, and T^{in}, for the ten selected modes. All of the values are scaled by the value of $\bar{T}^{\mathrm{in}}_{10}$, i.e., $\bar{T}^{\mathrm{in}}$ for A_g^{10} is set to 1.

Mode	$\bar{T}^{\mathrm{ec}}$	$\bar{T}^{\mathrm{ecSym}}$	$\bar{T}^{\mathrm{in}}$
B_{2g}^1	1.070	−0.030	0.294
B_g^2	0.822	−0.030	0.472
A_u^3	0.502	−0.018	0.385
B_{3u}^1	0.426	−0.008	0.104
B_{2g}^1	−0.035	−0.003	0.061
B_{1g}^6	0.497	−0.004	0.132
A_g^7	−0.045	−0.024	0.231
A_g^8	0.271	−0.014	0.214
A_g^9	0.695	−0.055	0.816
A_g^{10}	1.139	−0.062	1.000

Now we analyze the peak/dip of IETS for both the damped and undamped limits. From Fig. 8 we can see that the IETS shapes in the form of peaks in both the limiting cases. Since the transmission coefficient is much lower than 0.5 around the Fermi level, the 0.5 rule is satisfied for all the modes in both the damping limits. However, the relative intensities for each mode are different in the damped and undamped limits. For instance, let us focus on moieties of IETS, B_{2g}^1, (A_g^2, A_u^3, B_{3u}^4), (B_{1g}^6, A_g^7), and A_g^8, which are presented in Figs. 8(b) and 8(c). In the undamped limit, the peak intensities of these moieties are between 1 and 1.7 times larger that that of the A_g^8. On the other hand, in the damped limit, the moiety (A_g^2, A_u^3, B_{3u}^4) is much stronger than the A_g^8 (more than 3.5 times), and the peak height of the lowest B_{2g}^1 relative to that of A_g^8 also shows a large change (more than 2.5 times) when compared to the case of the damped limit. The above large difference of the relative IETS intensities between the damped and undamped limits is in striking contrast to the situation presented for the Au wire. In order to resolve this contradiction, we summarize the (normalized) transmission functions of the BDT/Au(001) system in Table II. Several features emerge from the table. First, the term $\bar{T}_\alpha^{\mathrm{ec}}$ is positive at the given bias for all the modes, but the values of the related $\bar{T}_\alpha^{\mathrm{ecSym}}$ are negative. Second, the absolute values of $\bar{T}_\alpha^{\mathrm{ecSym}}$ are much smaller than those of $\bar{T}_\alpha^{\mathrm{ec}}$ and $\bar{T}_\alpha^{\mathrm{in}}$, with the latter two terms being of the same order of magnitude. These features of the transmission functions are quite different from those of the Au wire, where $\bar{T}_\alpha^{\mathrm{ec}}$ and $\bar{T}_\alpha^{\mathrm{ecSym}}$ have almost the same negative values and dominate the IETS. In the present BDT/Au system, the inelastic terms ($\bar{T}_\alpha^{\mathrm{in}}$) domi-

nate the shape of IETS in the damped limit, but the elastic correction terms ($\bar{T}_\alpha^{\mathrm{ec}}$) give a similar contribution to the IETS in the undamped one. Therefore, the sets of IETS in the two limiting cases originate from a somewhat different structure of their relative intensities, although the positive sign of $\bar{T}_\alpha^{\mathrm{ec}}$ and small absolute value of $\bar{T}_\alpha^{\mathrm{ecSym}}$ ensure that the final result always complies with the 0.5 rule. As described in Sec. IV A, the large difference between $\bar{T}_\alpha^{\mathrm{ec}}$ and $\bar{T}_\alpha^{\mathrm{ecSym}}$ means that the value of Re $G(E)$ is not negligible. However, further analysis is *not* straightforward because the present system is *not* a simple one-channel conductive system and the off-diagonal terms (in the MO basis) play an important role in determining the IETS of the asymmetric modes, i.e., the single-level model is not insightful. Unfortunately, it is difficult to establish a general propensity rule for the shape of the IETS in the present LOE framework because we do not have clear rules for determining the sign of $\bar{T}_\alpha^{\mathrm{ec}}$ or the relation of magnitudes for $\bar{T}_\alpha^{\mathrm{ecSym}}$ and $\bar{T}_\alpha^{\mathrm{in}}$. In absence of a strict rule for the multichannel case, a positive $\bar{T}_\alpha^{\mathrm{ec}}$ and negative $\bar{T}_\alpha^{\mathrm{ecSym}}$ provide the possibility for the shape of the IETS of each mode to change individually from a peak to a dip when going from the undamped to the damped limit. This is particularly true for the asymmetric modes.

V. SUMMARY AND CONCLUSIONS

In conclusion, we have developed the efficient MO approach for the self-consistent nonequilibrium Green's function method. The main improvements over our previous approach[13] can be summarized as follows: (i) an improved construction of the embedding potential matrix, (ii) the introduction of a correction factor for the density matrix associated with the EGF-SCF and the embedding potential, and (iii) a numerically accurate $O(N)$ method for calculating the self-energy matrices for the electrodes. As a test of these schemes, we have performed NEGF-DFT calculations for a Au 6 atom long wire connected to (001) Au electrodes. Our results have shown good agreement with the calculations obtained by the standard NEGF-DFT approach. In particular we wish to stress the benefit of the mentioned point (iii). The simple application of Damle's method[65] for the evaluation of the self-energy matrices sometimes gives seriously inaccurate results because of nonphysical waveguide effects (see Sec. III). Therefore the careful modeling of the electrodes self-energies is important, in particular, when incorporating the periodic boundary conditions.

By using the efficient MO approach, we have then performed *ab initio* calculations for the inelastic transport within the LOE formalism for e-ph coupling. We have adopted the conventional expression of the conductance and IETS by simplifying the rigorous expression for total currents relating the elastic and inelastic terms derived by Viljas *et al.*[26] *Ab initio* calculations of the conductance and the IETS have been performed for the two systems: a Au 4 atom long wire (high conductance) and a BDT molecule (low conductance) both attached to Au electrodes. These are good benchmarks of the 0.5 rule. In order to perform a systematic analysis, we have focused on their temperature dependence, differences between the damped and undamped limits, and the propensity of symmetry for the IETS.

In both systems, the 0.5 rule was satisfied for all the phonon modes, i.e., the shape of the IETS always presents dips for the Au wire ($0.5 \ll T_0 \sim 1.0$) and peaks for the BDT ($T_0 \sim 0.05 \ll 0.5$). In the former case, the elastic correction terms, which relate to background scattering arising from virtual-phonon excitation, dominate the shape (and the intensity) of the IETS. The temperature affects strongly the structure of the total IETS when the thermal damping is not negligible. Upon increasing the temperature, the shape of the IETS becomes broader, and the tail of the strongest IETS signal covers the other dips. Thus the temperature and coupling to bath modes in electrodes should be always considered when analyzing experimental IETS.

When the bridge is the BDT molecule, the dominant term in the IETS changes from being the inelastic term in the damped limit to a competition between elastic and inelastic terms in the undamped case. Hence, details of the structure of the IETS are slightly different between the two limiting cases. Our theoretical expression for the IETS gives a simple insight into these findings. It is known that omitting the elastic correction and bias-dependent nonequilibrium phonon distributions (vibrational heating) cannot describe the correct structure of the IETS such as the shape (peak/dip) and the relative intensities. However, several theoretical models have been successfully applied to the present BDT/Au system without including these corrections. Our calculations show that the contributions of the elastic corrections to the IETS signals are of the same sign (i.e., peak) and the same order of magnitude as the inelastic terms for all of the modes. As a result, the gross features of the IETS (shape, activity of the modes) in the undamped limit do not change drastically when compared to the damped limit. This is the main reason why the damped limit is useful for a general analysis of the IETS in the BDT/Au system. However, in general there are no fundamental reasons for the elastic corrections and inelastic terms always to have similar values, same order, and sign.

Finally, we comment on the symmetry properties of the BDT/Au system. In our study, the whole contact region maintains the D_{2h} symmetry (in the 0 bias limit); thus the calculated data are not affected by the locality of the projected MOs on the BDT molecule. First, all of the IETS signals relating to the totally symmetric modes (A_g) are active. This could be understood with a simplified model for e-ph coupling (molecular on-site Holstein model). Much more interesting are the asymmetric modes (i.e., modes not belonging to the A_g irreducible representation). Only out-of-plane asymmetric modes, which relate to the A_u or B_g representation in the C_{2h} point group, give sufficiently strong IETS signals in the low-bias regime. Hence, the propensity rules proposed by Troisi and Ratner[47,48] are satisfied. However, we emphasize that a straightforward generalization of their rule is not necessarily suitable because of the competition between the elastic corrections and inelastic terms plays an important role in determining the IETS signals. In particular, the IETS is modified strongly by nonthermal vibrational heating. One promising route to rationalize these results is an extension of the propensity rules based on the transmission

channels proposed by Gagliardi *et al.*[41] and Paulsson *et al.*,[73] although the simplicity of the rule is lost when compared with original simple rule proposed by Troisi and Ratner.[47,48] When one proceeds in this direction, the following two questions must be answered: (a) Is it possible to extend eigenchannel concept, which rules out *all* of transmission functions? (b) Is there a simple tendency to determine both the sign and relative intensity of the elastic correction terms?[21]

In summary, we have proposed an efficient *ab initio* scheme for calculating ballistic and inelastic transports in molecular (nanowire) junctions, and we have calculated the conductance and IETS for two typical high- and low-conductance systems. Focusing on the 0.5 rule and propensity of symmetry, we performed systematic calculations and a thorough analysis including the effects of nonthermal vibrational heating as well as virtual-phonon excitation. Further applications to other molecular systems and a more detailed analysis to extend the propensity rule are currently in progress.

ACKNOWLEDGMENTS

This research was supported by a Grant-in-aid for Scientific Research on Priority Area under Contracts No. 20027002 (H.N.) and No. 20038017 (H.N. and K.Y.) from the Ministry of Education, Culture, Sports, Science, and Technology of Japan. The authors thank the Computer Center of the Institute for Molecular Science for the use of computers. S.S. and A.R.R. would like to thank Science Foundation of Ireland for financial support.

APPENDIX: CONVENTIONAL LOE FORMS FOR TERMINAL CURRENTS

In this appendix, we provide a brief explanation on how to obtain the terminal currents for the elastic correction and inelastic term at the same computational cost as that for obtaining the ballistic current. The starting equations are the rigorous LOE (E1)–(E3) given in Ref. 26. The first approximation consists in replacing the phonon density with a sum of the delta functions

$$\rho_\alpha(\omega) = -\frac{1}{\pi}\mathrm{Im}\, D_\alpha(\omega) \approx \delta(\omega-\Omega_\alpha) - \delta(\omega+\Omega_\alpha). \tag{A1}$$

Then we can easily perform the integration over the phonon energy ω. From Eq. (E3) in Ref. 26, one can obtain the inelastic terminal current for the mode α as follows:

$$i_\alpha^{\mathrm{inel}}(E) = \frac{1}{\pi}T_{\alpha+}^{\mathrm{in}}\{N_\alpha(f_L - f_{R+}) - f_{R+}(1-f_L)\} + \frac{1}{\pi}T_{\alpha-}^{\mathrm{in}}\{N_\alpha(f_L - f_{R-}) - f_L(1-f_{R-})\}, \tag{A2}$$

where T_α^{in} is E dependent [see Eq. (18)] and $f_{L/R}$ is the Fermi distribution. The symbol + (−) in the lower subscript indicates that the energy E in the functions should be replaced with $E+\Omega_\alpha(E-\Omega_\alpha)$. Equation (A2) is greatly simplified when compared to Eq. (E3), but one needs twice as much computational effort to calculate $i_\alpha^{\mathrm{inel}}(E)$ than $i^0(E)$ for each α. Therefore, if many modes are required to model the inelastic transport, this form is still rather inconvenient. As long as the DOSs of the leads and (ballistic) transmission coefficient T_0 are smooth functions of E around $E\sim\Omega_\alpha$, e.g., the following condition:

$$\left|\frac{T_0(E\pm\Omega_\alpha)-T_0(E)}{T_0(E)}\right| \lesssim 1 \tag{A3}$$

is satisfied in the energy range $|E-E_F|\le V_b$, we can approximate $T_{\alpha\pm}^{\mathrm{in}}$ to T_α^{in} and expect that the dominant energy exchange is contained in the coexistence of the shifted Fermi functions, f and $f_\pm$. Thus one can obtain

$$\begin{aligned} i_\alpha^{\mathrm{inel}}(E) &\approx \frac{1}{\pi}T_\alpha^{\mathrm{in}}\{N_\alpha(2f_L - f_{R+} - f_{R-}) \\ &\quad - f_{R+}(1-f)_L + f_L(1-f_{R-})\} \\ &\approx \frac{1}{\pi}T_\alpha^{\mathrm{in}}\{2N_\alpha(f_L - f_R) + f_{R+}(1-f_L) + f_L(1-f_{R-})\}. \end{aligned} \tag{A4}$$

Because evaluating the values of $f_{R\pm}$ is an easy task and the α dependence of T_α^{in} is now reduced only to that contained in the $\mathbf{M}^\alpha$ matrix, the inelastic terminal current can be obtained simultaneously with the ballistic current. The total inelastic terminal current $i^{\mathrm{inel}}(E)$ is represented by $\Sigma_\alpha i_\alpha^{\mathrm{inel}}(E)$.

The elastic correction term for mode α can be further separated into the three terms $i_\alpha^{\mathrm{ec}}(E)$, $i_\alpha^{\mathrm{ec}L}(E)+i_\alpha^{\mathrm{ec}R}(E)$, and an asymmetric correction $i_\alpha^{\mathrm{asym}}(E)$; the last term relating to the principal part integral for the real part of the phonon Green's function. In the present form, we omit the asymmetric term (i.e., the principal integral part). This is a good approximation if the E-M-E system consists of symmetric electrodes. Following a similar procedure to that used to derive Eq. (A4), we obtain

$$\begin{aligned} i_\alpha^{\mathrm{ec}}(E) &\approx \frac{1}{\pi}\{T_{\alpha+}^{\mathrm{ec}}N_\alpha(f_L - f_R) + T_{\alpha-}^{\mathrm{ec}}(N_\alpha+1)(f_L - f_R)\} \\ &\approx \frac{1}{\pi}T_\alpha^{\mathrm{ec}}(2N_\alpha+1)(f_L - f_R), \end{aligned} \tag{A5}$$

$$\begin{aligned} i_\alpha^{\mathrm{ec}L}(E) + i_\alpha^{\mathrm{ec}L}(E) &\approx \frac{1}{\pi}\{(T_{\alpha+}^{\mathrm{ec}L}f_{L+} + T_{\alpha+}^{\mathrm{ec}R}f_{R+})(f_L - f_R) \\ &\quad - (T_{\alpha-}^{\mathrm{ec}L}f_{L-} + T_{\alpha-}^{\mathrm{ec}R}f_{R-})(f_L - f_R)\} \\ &\approx \frac{2}{\pi}\{T_\alpha^{\mathrm{ec}L}(f_{L+} - f_{L-})(f_L - f_R) \\ &\quad + T_\alpha^{\mathrm{ec}R}(f_{R+} - f_{R-})(f_L - f_R)\}, \end{aligned} \tag{A6}$$

where the transmission coefficient-type function T_α^{ec} is given in Eq. (16) and $T_\alpha^{\mathrm{ec}L/R}$ are

$$T_\alpha^{\mathrm{ec}L/R}(E) = \mathrm{Im\ Tr}[\mathbf{M}^\alpha \mathbf{G}_{CC}^0(E)\mathbf{\Gamma}_{L/R}(E + V_b/2)\mathbf{G}_{CC}^{0\dagger}(E)\mathbf{M}^\alpha \mathbf{G}_{CC}^0(E)\mathbf{\Gamma}_{R/L}(E - V_b/2)\mathbf{G}_{CC}^{0\dagger}(E)\mathbf{\Gamma}_{L/R}(E + V_b/2)\mathbf{G}_{CC}^0(E)]. \tag{A7}$$

The elastic correction terminal currents $\delta i^{\mathrm{el}}(E)$ is expressed as

$$\delta i_\alpha^{\mathrm{el}}(E) = \frac{1}{\pi}\{T_\alpha^{\mathrm{ec}}(2N_\alpha + 1)(f_L - f_R) + 2T_\alpha^{\mathrm{ec}L}(f_{L+} - f_{L-})(f_L - f_R) + 2T_\alpha^{\mathrm{ec}R}(f_{R+} - f_{R-})(f_L - f_R)\}. \tag{A8}$$

The total elastic correction is the sum over the α, i.e., $\delta i^{\mathrm{ec}}(E) = \Sigma_\alpha \delta i_\alpha^{\mathrm{ec}}(E)$ and can be estimated simultaneously with the ballistic current just as with the inelastic term. If one needs each terminal current, Eq. (A8) is the final result of our conventional LOE. When only the (integrated) currents and IETS signals are required, more simplifications are possible. Since the transmission functions are smooth functions of E in our assumption, the integrals over E for the above terminal currents may be separated into the averaged transmission functions and an analytical integral of the remaining Fermi functions. In this respect, the various T functions are replaced to the average $\bar{T}$. With noting the assumption that the DOS, etc. are smooth function of E and the leads are symmetric, the averages over E, $\bar{T}_\alpha^{\mathrm{ec}L/R}$ can be approximated as

$$\bar{T}_\alpha^{\mathrm{ec}L/R} \approx \frac{1}{2}\bar{T}_\alpha^{\mathrm{ecSym}}(E) = \frac{1}{2}(\bar{T}_\alpha^{\mathrm{ec}L} + \bar{T}_\alpha^{\mathrm{ec}R}), \tag{A9}$$

where the term $T_\alpha^{\mathrm{ecSym}}$ has been introduced in Eq. (17). Note that the integrals contain the factor $(f_L - f_R)$, thus the average should be carried out in a convenient range around $[\mu_L, \mu_R]$. Then we finally arrive at the expression for the conductance and current given in Eqs. (13) and (14).

In order to obtain the phonon distribution function N_α, one needs similar expressions for the self-energies of the phonons and this is possible by using the same approximations described above. The only difference is that the self-energies do not contain the factor $(f_L - f_R)$ explicitly; thus the E dependence of the resulting transmission functions such as T_α^{eh} should be approximated by the values at $E = E_F$ instead of the average. As a result, the additional computational cost to evaluate N_α is negligible.

*Corresponding author; nakamura@tcl.t.u-tokyo.ac.jp

[1] D. M. Adams, L. Brus, C. E. D. Chidsey, S. Creager, C. Creutz, C. R. Kagan, P. V. Kamat, M. Lieberman, S. Lindsay, R. A. Marcus, R. M. Metzger, M. E. Michel-Beyerle, J. R. Miller, M. D. Newton, D. R. Rolison, O. Sankey, K. S. Schanze, J. Yardley, and X. Y. Zhu, J. Phys. Chem. B **107**, 6668 (2003).

[2] N. Agrait, C. Untiedt, G. Rubio-Bollinger, and S. Vieira, Phys. Rev. Lett. **88**, 216803 (2002).

[3] M. A. Reed, C. Zhou, M. R. Deshpande, C. J. Muller, T. P. Burgin, L. Jones, and J. M. Tour, Ann. N.Y. Acad. Sci. **852**, 133 (1998).

[4] M. A. Reed, C. Zhou, C. J. Muller, T. P. Burgin, and J. M. Tour, Science **278**, 252 (1997).

[5] J. Chen, M. A. Reed, A. M. Rawlett, and J. M. Tour, Science **286**, 1550 (1999).

[6] J. Chen, W. Wang, J. Klemic, M. A. Reed, B. W. Axelrod, D. M. Kaschak, A. M. Rawlett, D. W. Price, S. M. Dirk, J. M. Tour, D. S. Grubisha, and D. W. Bennett, Ann. N.Y. Acad. Sci. **960**, 69 (2002).

[7] S. Sen and S. Chakrabarti, J. Phys. Chem. C **112**, 1685 (2008).

[8] V. Mujica, M. Kemp, and M. A. Ratner, J. Chem. Phys. **101**, 6849 (1994).

[9] A. Nitzan and M. A. Ratner, Science **300**, 1384 (2003).

[10] M. Brandbyge, J. L. Mozos, P. Ordejon, J. Taylor, and K. Stokbro, Phys. Rev. B **65**, 165401 (2002).

[11] P. Damle, A. W. Ghosh, and S. Datta, Chem. Phys. **281**, 171 (2002).

[12] T. Frederiksen, M. Paulsson, M. Brandbyge, and A. P. Jauho, Phys. Rev. B **75**, 205413 (2007).

[13] H. Nakamura and K. Yamashita, J. Chem. Phys. **125**, 194106 (2006).

[14] A. R. Rocha, V. M. Garcia-Suarez, S. Bailey, C. Lambert, J. Ferrer, and S. Sanvito, Phys. Rev. B **73**, 085414 (2006).

[15] K. Stokbro, J. Taylor, M. Brandbyge, and P. Ordejon, Ann. N.Y. Acad. Sci. **1006**, 212 (2003).

[16] J. Taylor, H. Guo, and J. Wang, Phys. Rev. B **63**, 245407 (2001).

[17] C. Toher and S. Sanvito, Phys. Rev. Lett. **99**, 056801 (2007).

[18] Y. Q. Xue, S. Datta, and M. A. Ratner, Chem. Phys. **281**, 151 (2002).

[19] J. R. Reimers, G. C. Solomon, A. Gagliardi, A. Bilic, N. S. Hush, T. Frauenheim, A. Di Carlo, and A. Pecchia, J. Phys. Chem. A **111**, 5692 (2007).

[20] N. Agrait, C. Untiedt, G. Rubio-Bollinger, and S. Vieira, Chem. Phys. **281**, 231 (2002).

[21] J. M. Beebe, H. J. Moore, T. R. Lee, and J. G. Kushmerick, Nano Lett. **7**, 1364 (2007).

[22] L. de la Vega, A. Martin-Rodero, N. Agrait, and A. L. Yeyati, Phys. Rev. B **73**, 075428 (2006).

[23] T. Frederiksen, M. Brandbyge, N. Lorente, and A. P. Jauho, Phys. Rev. Lett. **93**, 256601 (2004).

[24] M. Galperin, M. A. Ratner, and A. Nitzan, J. Phys.: Condens. Matter **19**, 103201 (2007).

[25] M. Paulsson, T. Frederiksen, and M. Brandbyge, Phys. Rev. B **72**, 201101 (2005) R.

[26] J. K. Viljas, J. C. Cuevas, F. Pauly, and M. Hafner, Phys. Rev. B **72**, 245415 (2005).

[27] T. Frederiksen, N. Lorente, M. Paulsson, and M. Brandbyge, Phys. Rev. B **75**, 235441 (2007).

[28] W. Ho, J. Chem. Phys. **117**, 11033 (2002).

[29] M. Kawai, T. Komeda, Y. Kim, Y. Sainoo, and S. Katano, Philos. Trans. R. Soc. London, Ser. A **362**, 1163 (2004).

[30] N. Lorente and M. Persson, Phys. Rev. Lett. **85**, 2997 (2000).

[31] N. Lorente, M. Persson, L. J. Lauhon, and W. Ho, Phys. Rev. Lett. **86**, 2593 (2001).

[32] H. Ness and A. J. Fisher, Proc. Natl. Acad. Sci. U.S.A. **102**, 8826 (2005).
[33] A. Troisi and M. A. Ratner, Phys. Rev. B **72**, 033408 (2005).
[34] B. C. Stipe, M. A. Rezaei, and W. Ho, Science **280**, 1732 (1998).
[35] H. Ueba, T. Mii, and S. G. Tikhodeev, Surf. Sci. **601**, 5220 (2007).
[36] S. Alavi, B. Larade, J. Taylor, H. Guo, and T. Seideman, Chem. Phys. **281**, 293 (2002).
[37] Y. Kim, T. Komeda, and M. Kawai, Phys. Rev. Lett. **89**, 126104 (2002).
[38] A. J. Mayne, G. Dujardin, G. Comtet, and D. Riedel, Chem. Rev. **106**, 4355 (2006).
[39] G. P. Salam, M. Persson, and R. E. Palmer, Phys. Rev. B **49**, 10655 (1994).
[40] S. Datta, *Electronic Transport in Mesoscopic Systems* (Cambridge University Press, Cambridge, 1995).
[41] A. Gagliardi, G. C. Solomon, A. Pecchia, T. Frauenheim, A. Di Carlo, N. S. Hush, and J. R. Reimers, Phys. Rev. B **75**, 174306 (2007).
[42] H. Ness, J. Phys.: Condens. Matter **18**, 6307 (2006).
[43] D. A. Ryndyk, M. Hartung, and G. Cuniberti, Phys. Rev. B **73**, 045420 (2006).
[44] M. Paulsson, T. Frederiksen, and M. Brandbyge, Nano Lett. **6**, 258 (2006).
[45] A. Troisi, J. M. Beebe, L. B. Picraux, R. D. van Zee, D. R. Stewart, M. A. Ratner, and J. G. Kushmerick, Proc. Natl. Acad. Sci. U.S.A. **104**, 14255 (2007).
[46] Y. Asai, Phys. Rev. Lett. **93**, 246102 (2004).
[47] A. Troisi and M. A. Ratner, J. Chem. Phys. **125**, 214709 (2006).
[48] A. Troisi and M. A. Ratner, Nano Lett. **6**, 1784 (2006).
[49] N. S. Wingreen, A. P. Jauho, and Y. Meir, Phys. Rev. B **48**, 8487 (1993).
[50] A. P. Jauho, N. S. Wingreen, and Y. Meir, Phys. Rev. B **50**, 5528 (1994).
[51] R. Landauer, Philos. Mag. **21**, 863 (1970).
[52] A. Nitzan, J. Phys. Chem. A **105**, 2677 (2001).
[53] T. Holstein, Ann. Phys. **8**, 343 (1959).
[54] N. Sergueev, D. Roubtsov, and H. Guo, Phys. Rev. Lett. **95**, 146803 (2005).
[55] S. H. Ke, H. U. Baranger, and W. T. Yang, J. Chem. Phys. **123**, 114701 (2005).
[56] S. H. Ke, H. U. Baranger, and W. T. Yang, J. Comput. Theor. Nanosci. **3**, 819 (2006).
[57] H. Nakamura, J. Phys.: Condens. Matter **20**, 224023 (2008).
[58] H. Nakamura and K. Yamashita, Nano Lett. **8**, 6 (2008).
[59] S. Sanvito, C. J. Lambert, J. H. Jefferson, and A. M. Bratkovsky, Phys. Rev. B **59**, 11936 (1999).
[60] K. S. Thygesen and K. W. Jacobsen, Phys. Rev. B **72**, 033401 (2005).
[61] I. Rungger and S. Sanvito, Phys. Rev. B **78**, 035407 (2008).
[62] M. Galperin and A. Nitzan, Ann. N.Y. Acad. Sci. **1006**, 48 (2003).
[63] B. O. Roos and P. R. Taylor, Chem. Phys. **48**, 157 (1980).
[64] K. Ruedenberg, M. W. Schmidt, M. M. Gilbert, and S. T. Elbert, Chem. Phys. **71**, 41 (1982).
[65] P. S. Damle, A. W. Ghosh, and S. Datta, Phys. Rev. B **64**, 201403 (2001).
[66] A. R. Rocha, V. M. Garcia-Suarez, S. W. Bailey, C. J. Lambert, J. Ferrer, and S. Sanvito, Nat. Mater. **4**, 335 (2005).
[67] J. P. Perdew, K. Burke, and M. Ernzerhof, Phys. Rev. Lett. **77**, 3865 (1996).
[68] L. Kleinman and D. M. Bylander, Phys. Rev. Lett. **48**, 1425 (1982).
[69] J. M. Soler, E. Artacho, J. D. Gale, A. Garcia, J. Junquera, P. Ordejon, and D. Sanchez-Portal, J. Phys.: Condens. Matter **14**, 2745 (2002).
[70] V. M. Garcia-Suarez, T. Kostyrko, S. Bailey, C. Lambert, and B. R. Bulka, Phys. Status Solidi B, **244**, 2443 (2007).
[71] K. Stokbro, J. Taylor, M. Brandbyge, J. L. Mozos, and P. Ordejon, Comput. Mater. Sci. **27**, 151 (2003).
[72] C. Toher and S. Sanvito, Phys. Rev. B **77**, 155402 (2008).
[73] M. Paulsson, T. Frederiksen, H. Ueba, N. Lorente, and M. Brandbyge, Phys. Rev. Lett. **100**, 226604 (2008).